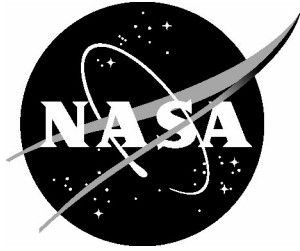


NASA/TM-2004-213018



Meteorology and Wake Vortex Influence on American Airlines FL-587 Accident

*Fred H. Proctor, David W. Hamilton, and David K. Rutishauser
Langley Research Center, Hampton, Virginia*

*George F. Switzer
Research Triangle Institute, Hampton, Virginia*

April 2004

The NASA STI Program Office . . . in Profile

Since its founding, NASA has been dedicated to the advancement of aeronautics and space science. The NASA Scientific and Technical Information (STI) Program Office plays a key part in helping NASA maintain this important role.

The NASA STI Program Office is operated by Langley Research Center, the lead center for NASA's scientific and technical information. The NASA STI Program Office provides access to the NASA STI Database, the largest collection of aeronautical and space science STI in the world. The Program Office is also NASA's institutional mechanism for disseminating the results of its research and development activities. These results are published by NASA in the NASA STI Report Series, which includes the following report types:

- **TECHNICAL PUBLICATION.** Reports of completed research or a major significant phase of research that present the results of NASA programs and include extensive data or theoretical analysis. Includes compilations of significant scientific and technical data and information deemed to be of continuing reference value. NASA counterpart of peer-reviewed formal professional papers, but having less stringent limitations on manuscript length and extent of graphic presentations.
- **TECHNICAL MEMORANDUM.** Scientific and technical findings that are preliminary or of specialized interest, e.g., quick release reports, working papers, and bibliographies that contain minimal annotation. Does not contain extensive analysis.
- **CONTRACTOR REPORT.** Scientific and technical findings by NASA-sponsored contractors and grantees.

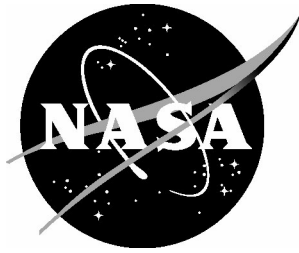
- **CONFERENCE PUBLICATION.** Collected papers from scientific and technical conferences, symposia, seminars, or other meetings sponsored or co-sponsored by NASA.
- **SPECIAL PUBLICATION.** Scientific, technical, or historical information from NASA programs, projects, and missions, often concerned with subjects having substantial public interest.
- **TECHNICAL TRANSLATION.** English-language translations of foreign scientific and technical material pertinent to NASA's mission.

Specialized services that complement the STI Program Office's diverse offerings include creating custom thesauri, building customized databases, organizing and publishing research results ... even providing videos.

For more information about the NASA STI Program Office, see the following:

- Access the NASA STI Program Home Page at <http://www.sti.nasa.gov>
- E-mail your question via the Internet to help@sti.nasa.gov
- Fax your question to the NASA STI Help Desk at (301) 621-0134
- Phone the NASA STI Help Desk at (301) 621-0390
- Write to:
NASA STI Help Desk
NASA Center for AeroSpace Information
7121 Standard Drive
Hanover, MD 21076-1320

NASA/TM-2004-213018



Meteorology and Wake Vortex Influence on American Airlines FL-587 Accident

*Fred H. Proctor, David W. Hamilton, and David K. Rutishauser
Langley Research Center, Hampton, Virginia*

*George F. Switzer
Research Triangle Institute, Hampton, Virginia*

National Aeronautics and
Space Administration

Langley Research Center
Hampton, Virginia 23681-2199

April 2004

Available from:

NASA Center for Aerospace Information (CASI)
7121 Standard Drive
Hanover, MD 21076-1320
(301) 621-0390

National Technical Information Service (NTIS)
5285 Port Royal Road
Springfield, VA 22161-2171
(703) 605-6000

Table of Contents

Table of Contents.....	iii
List of Figures.....	v
List of Tables.....	vii
ABSTRACT.....	1
1.0 Introduction.....	3
1.1 Weather Conditions at JFK.....	3
1.2 Accident Synopsis.....	3
2.0 Aircraft Wake Vortices.....	4
2.1 Background.....	4
2.2 History of Wake Vortex Research at Langley.....	7
3.0 Analysis of Ambient Conditions.....	7
3.1 Ambient Wind Profiles.....	9
3.2 Ambient Temperature Profile.....	9
3.3 Analysis of Wind Profiles from JAL 47.....	9
3.4 Analysis of Environmental Turbulence.....	11
4.1 Initial Parameters for Generating Aircraft.....	12
4.2 Environmental Parameters.....	13
5.0 Model Predictions for Wake Vortex Strength and Drift.....	13
5.1 APA Predictions.....	13
5.1.1 Initialization.....	14
5.1.2 Approach.....	14
5.1.3 Suspected First-Encounter Region.....	14
5.2 TDAWP Predictions.....	17
5.3 Three-Dimensional TASS Predictions.....	17
5.3.1 Model Domain.....	18
5.3.1 Initialization Parameters.....	19
5.3.2 Three-Dimensional TASS Results.....	19
6.0 TASS Model Data Sets.....	21
6.1 Discretized data sets.....	21
6.2 Simple model fit.....	21
6.3 Algebraic model for wake vortex wind field.....	23
7.0 Summary and Conclusions.....	25
8.0 Acknowledgements.....	27
Appendix-A. TDAWP: TASS Driven Algorithms for Wake Prediction.....	28
Model Concept.....	28
TASS Parametric Cases.....	29
TASS Domain, Boundary, and Initial Conditions.....	29
Determination of Vortex Position and Circulation.....	31
Predictive Model Development.....	31
Vortex Transport Model.....	31
Vortex Hazard Model.....	34
Predictive Model Comparisons with TASS.....	36
Verification of TDAWP with Field Measurements.....	40
Summary.....	41

Appendix-B. Description of TASS.....	44
References.....	46

List of Figures

Figure 1. Plan view of JFK Airport with flight paths for JAL 47 and AA 587.	4
Figure 2. Aircraft wake vortices in relation to generating aircraft (viewed from below).	5
Figure 3. Comparison of measurements for atmospheric wind speed and direction at time of accident (source NTSB ¹).	8
Figure 4. Ambient atmospheric temperature vs altitude from JAL 47.	9
Figure 5. Wind profile from JAL 47.	10
Figure 6. Same as fig 5, but wind components relative to the 203 degree heading of AA 587. Crosswind component is denoted by blue curve.	10
Figure 7. Vertical shear of the crosswind component (blue curve). The second derivative of the crosswind is shown by the blue curve.	11
Figure 8. Turbulence eddy dissipation rate as a function of altitude.	12
Figure 9. Plan view of aircraft trajectories and wake vortex positions at time of first suspected wake encounter.	15
Figure 10. Vertical cross section at location of AA 587 at time of first apparent wake encounter (viewed from south).	15
Figure 11. Same as fig 9, but at time of second apparent wake encounter.	16
Figure 12. Same as fig 10, but at time of second apparent wake encounter.	16
Figure 13. Three-dimensional perspective of simulated JAL 47 wake vortex at time of encounter.	20
Figure 14. Simulated contour fields of velocity at time of encounter (100 seconds).	22
Figure 15. Same as fig 14, but for wind vector field.	22
Figure 16. Simple model fit to TASS wake vortex at 100 seconds.	23
Figure 17. Coordinates for algebraic model fit of AA 587 vortex system.	24
Figure 18. Three-dimensional projection of vortex pair from proposed algebraic model (with $C_1=0$).	26
Figure 19. Profile of vertical velocity (w) and lateral velocity (v) along a flight path located at $z=5m$, $y=25m$. Change in velocities due to sinusoidal oscillation of vortex center.	26
Figure A- 1. Wake vortex time to link vs turbulence intensity.	32
Figure A- 2. Comparison of TDAWP predictive model for transport to TASS results for neutral stratification. The symbols and the lines with symbols refer to TASS and the predictive model, respectively.	37
Figure A- 3. Same as fig A-2, but for the weak turbulence intensity level.	37
Figure A- 4. Same as fig A-3, but for the moderate turbulence intensity level.	38
Figure A- 5. Comparison of TDAWP predictive model for hazard to TASS results for neutral stratification. The symbols and the lines with symbols refer to TASS and the predictive model, respectively.	38
Figure A- 6. Same as fig A-5, but for the weak turbulence intensity level.	39
Figure A- 7. Same as fig A-6, but for the moderate turbulence intensity level.	39
Figure A- 8. Comparison between TDAWP model predictions and Memphis field data for circulation vs time. Squares represent LIDAR estimates of port vortex while triangles represent starboard.	42

Figure A- 9. Comparison between TDAWP predictions and Memphis field data for altitude vs time. Squares represent LIDAR measurements of port vortex while triangles represent starboard vortex.....43

List of Tables

Table 1. Salient Characteristics of TASS.	18
Table A- 1. Ambient stratification levels used for the predictive model development.....	30
Table A- 2. Ambient turbulence intensity levels used for the predictive model development. ..	30
Table A- 3. Stratification and turbulence intensity levels used for the predictive model development.....	30
Table A- 4. Description of cases used from Memphis field study.	40
Table B- 1. TASS History	44

ABSTRACT

The atmospheric environment surrounding the crash of American Airlines Flight 587 is investigated. Examined are evidence for any unusual atmospheric conditions and the potential for encounters with aircraft wake vortices. Computer simulations are carried out with two different vortex prediction models and a Large Eddy Simulation model. Wind models are proposed for studying aircraft and pilot response to the wake vortex encounter.

1.0 Introduction

On November 12, 2001, an Airbus A300-600 crashed shortly after takeoff from John F Kennedy (JFK) Airport, killing all 260 people on board as well as 5 people on the ground. The crash occurred at approximately 9:16 AM EST (1416 UTC), after traveling only 7.5 *km* (4 *NM*) from the end of runway 31L. The American Airlines jetliner was on a routine flight to Santo Domingo, Dominican Republic. In this report, weather conditions and wake turbulence are examined for possible contributing factors in this tragic event. Other information regarding this accident investigation can be found at the National Transportation Safety Board's (NTSB) web site.¹

1.1 Weather Conditions at JFK

A high pressure covering the eastern half of the United States had pushed a cold front through the New York City area the previous day. The weather conditions associated with this airmass were typical for that time of year: mostly clear skies, seasonably cool temperatures, and a gentle northwest breeze.

Fair skies and good visibility with Visual Meteorological Conditions (VMC) existed at JFK during the time of the accident. Measurements from an Automated Surface Observing System (ASOS) indicated surface wind speeds between 4-5 *m/s* (8-11 knots) from a direction ranging between 270-310 degrees. The surface temperature was reported as 6 °C, and a few isolated clouds were estimated at 1300 *m* (4300 *ft*). Examination of weather data from the FAA's Integrated Terminal Weather System (ITWS)^{2,3} and two regional weather prediction models^{4,5} indicated that a wind direction from the northwest was predominate between the surface and 1500 *m* (5000 *ft*). Also, these sources indicated a morning-time convective boundary layer that was capped by dry, stable conditions aloft. Any weather phenomenology that was atypical or that could adversely affect aircraft operations at JFK was not obvious from analysis of the observed and model forecast data. There were no reports of aircraft turbulence or other notable weather activity prior to the time of the accident.

1.2 Accident Synopsis

American Airlines Flight 587 (AA 587) began its takeoff roll at approximately one minute and 40 seconds after Japan Airlines 47 (JAL 47), a Boeing 747-400, departed the same runway. The flight path of AA 587 was about 1300 *m* (0.7 *NM*) east and 245 *m* (800 *ft*) below that of JAL 47 (fig 1). The flight path of AA 587 was lower and downwind from that of JAL 47, and thus was at risk from the wake vortices generated by the heavy B-747.

Preliminary assessments by the National Transportation Safety Board (NTSB) have indicated two possible wake turbulence encounters.¹ These suspected encounters were associated with sudden accelerations recorded by the AA 587 flight data recorder (FDR). The first suspected encounter occurred at 9:15:35 EST, about 66 *sec* following liftoff, when the aircraft was 535 *m* (1750 *ft*) above the ground. At this point, the aircraft experienced some minor lateral and vertical

accelerations and an initial roll to starboard (right). Several seconds later the pilot voiced a comment about a “wake turbulence encounter.” The second suspected encounter occurred at approximately 9:15:51 EST, some 82 *sec* after liftoff. By this time the aircraft had reached an altitude of 740 *m* (2430 *ft*) and was maintaining an air speed of 240 knots (122 *m/s*). The suspected encounter began as AA 587 experienced minor vertical and lateral accelerations and an initial roll to port (left). This encounter began 10 *sec* before the end of FDR data and 21 *sec* before ground impact. During the last 9 *sec* of FDR data, the aircraft experienced three strong lateral oscillations that corresponded to rudder movements. This was followed by a loss of control as critical components of the tail failed and departed the aircraft. In the 11 *sec* following the end of the FDR data, the aircraft plunged to the ground.

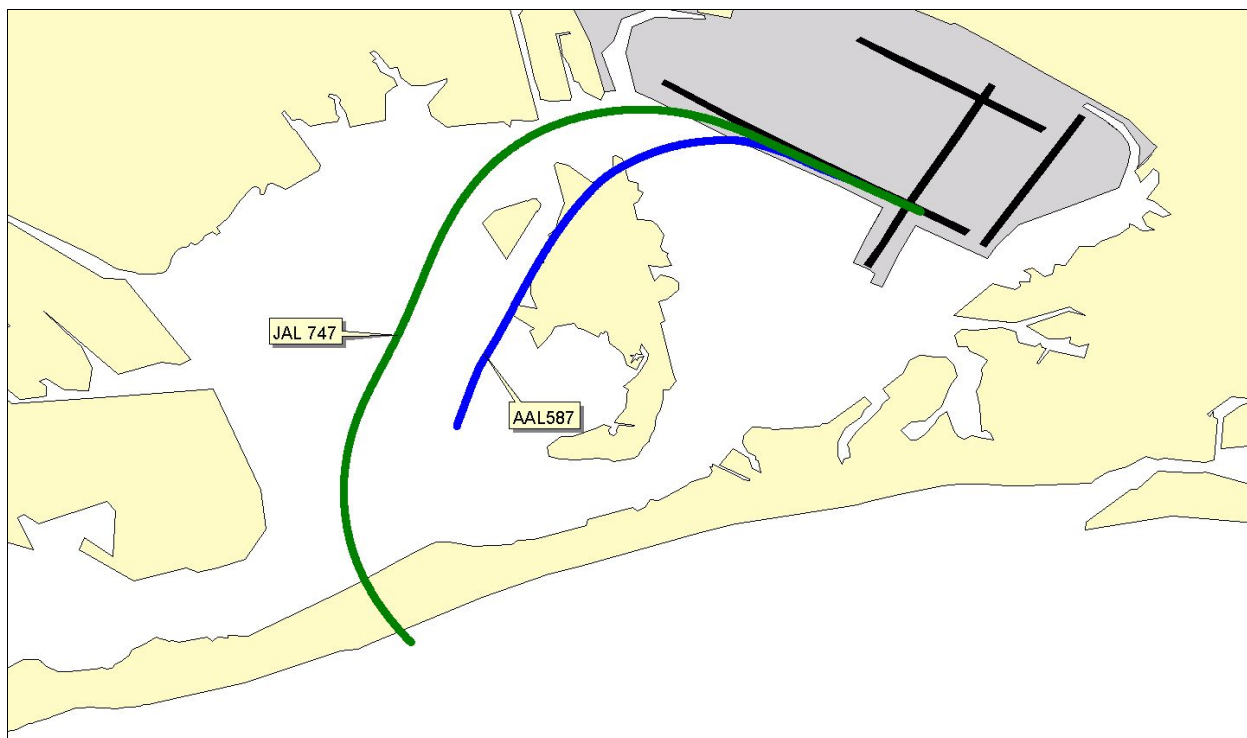


Figure 1. Plan view of JFK Airport with flight paths for JAL 47 and AA 587.

Both AA 587 and JAL 47 weighed over 255,000 *lbs*, and thus are grouped into the FAA’s “heavy” class of aircraft. Safety standards require that heavy’s maintain either a 4 *NM* or a 2 minute separation on single runway departures.^{6,7} This separation standard of 4 *NM* was not violated by AA 587 prior to the crash.

2.0 Aircraft Wake Vortices

2.1 Background

While an aircraft is in flight, trailing vortices are formed due to lift over the wings and flaps. Several spans downstream, these vortices merge into a pair of prominent counter-rotating

vortices that trail along the aircraft's path (fig 2). The initial size and intensity of these vortices depends on parameters of the generating aircraft such as wingspan, weight, and airspeed. The initial circulation of the wake vortices is proportional to weight, while being inversely proportional to airspeed and wingspan. In general, the wake vortices sink downward behind the generating aircraft. A crosswind will cause the wake vortices to drift laterally away from the flight path. Distortions in the path of the vortex can occur some distance downstream, due to self-induced instabilities and due to differential transport by atmospheric eddies and thermals. The strength of the wake vortices diminishes with distance downstream from the generating aircraft. Atmospheric and aircraft parameters determine the rate at which the vortices decay. Linking between the vortex pair to form crude vortex rings may occur some distance behind the generating aircraft. This linking called Crow instability,⁸ is associated with a rapid decrease in vortex circulation.

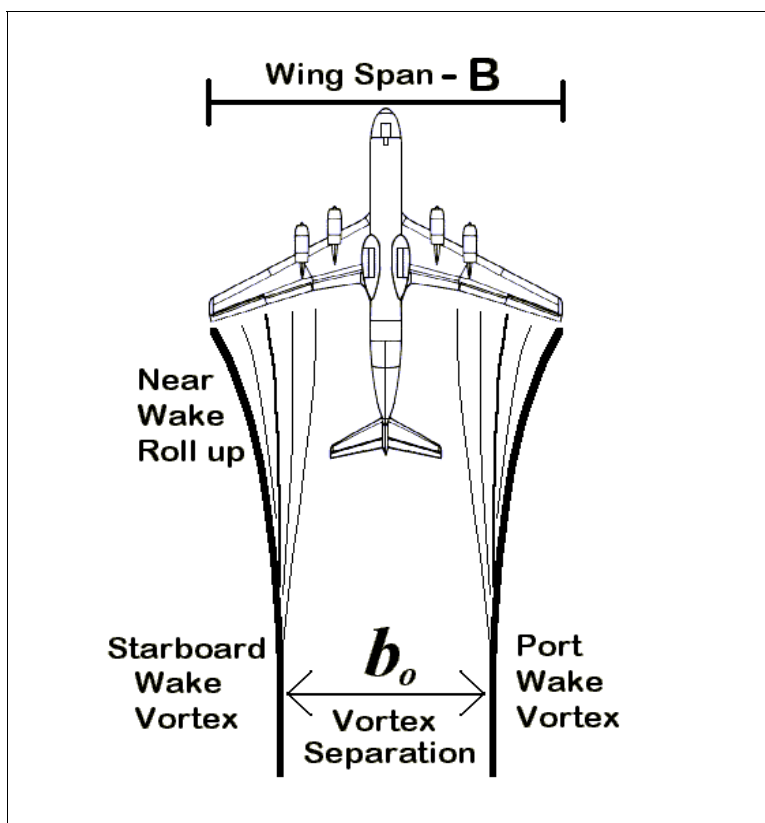


Figure 2. Aircraft wake vortices in relation to generating aircraft (viewed from below).

In-flight encounters with wake vortices, sometimes referred to as *wake turbulence*, is known to be hazardous especially for smaller aircraft behind larger aircraft. In-trail encounters with wake vortices may result in rolling moments, unexpected lateral and vertical loads, a loss of lift, and a loss of control authority. For safety, Air Traffic Control (ATC) employs a minimum separation that must be maintained by aircraft while in-flight.⁶ These separation standards have been empirically determined and are based on weight categories of both leading and following aircraft.

The hazard resulting from a wake vortex encounter depends on the strength of the vortex, and the span of the encountering aircraft.⁹ Heavy aircraft generate wakes with stronger circulations than do smaller aircraft. Thus for safety, larger spacings are required for smaller aircraft in-trail of heavy aircraft. Another factor that may contribute to the hazard is the geometry of the wake vortex encounter. Brief encounters may only be sensed as turbulence while sustained encounters may result in upsets. The most dangerous time for a wake encounter is during take-offs and landings. Here an aircraft encountering a wake vortex has little altitude to recover from either an upset or a loss of lift. Accidents due to wake encounters by heavy aircraft are rare. Most wake vortex accidents occur when smaller aircraft encounter the wakes of larger aircraft. Reports of structural damage attributed directly to a wake encounter are very rare.

Peak tangential wind speeds at the core of wake vortices can exceed 40 m/s.^{10,11} However, the most intense wind speeds are confined to vortex diameters less than one or two meters,¹¹ a scale that is much less than the diameter of an airliner fuselage.

The hazard resulting from a wake vortex encounter is best estimated by vortex circulation rather than peak tangential velocity. The high velocity near the vortex core is less important in contributing to aircraft roll than the integrated flowfield across the span of the encountering aircraft. The average circulation[†] has been shown to be correlated with aircraft roll rate.¹² Hinton and Tatnall¹³ evaluated several parameters, and found the average circulation between $r = 5$ and 15 m to be a representative metric for estimating hazard. Note that this hazard definition assumes a certain magnitude of un-commanded roll, and is not dependent upon aircraft type and encounter geometry. A wake hazard definition accepted with consensus by the stakeholder community currently does not exist.

Current FAA spacing metrics do not consider the influence of atmospheric conditions, although ambient wind flow, thermal stratification, and turbulence are known to affect wake vortex decay and transport. Current standards, which are based on aircraft weight only, are thought to be overly conservative.¹⁴

Aircraft wake vortices decay with time or distance downstream from the generating aircraft. The lifetime of the vortex depends upon its initial strength as well as the ambient weather conditions. Some characteristics of wake vortex decay are as follows:

- Lifetime of aircraft wake vortices are from 15 seconds to several minutes;
- Wake vortices have the longest lifetime within environments having weak turbulence and near-neutral thermal stratification;
- Aircraft wake vortices decay primarily due to influences of:
 - Intensity of ambient turbulence (eddy dissipation rate - ϵ)
 - Magnitude of thermal stratification (Brunt-Vaisala frequency - N)
 - Ground interaction
 - Three-dimensional instabilities;

[†] In a given cross sectional plane, the average circulation between radii $r=a$ and $r=b$ is defined

as $\bar{\Gamma}^{ab} = \frac{\int_a^b \Gamma_r dr}{\int_a^b dr}$, where Γ_r is the circulation at radius r from the vortex center.

- Rapid vortex decay usually follows the onset of three-dimensional sinusoidal instabilities:
 - Two forms: long-wave instability (wavelength $\sim 4-9 b_o$); short-wave instability (wavelength $<3b_o$)
 - Onset time is a function of: aircraft parameters, ε , and N .

The transport of aircraft wake vortices also is dependent upon atmospheric conditions as well as parameters of the generating aircraft:

- Ambient turbulence and vortex instabilities may distort the wake vortex path;
- Above the influence of the ground, wake vortices are transported laterally with the wind, while sinking due to mutual induction of the vortex pair;
- The wake vortex sink rate is a function of the vortex circulation and aircraft span. Wake vortices from commercial jetliners sink initially at a speed of 1-3 *m/s*;
- The sink rate decrease as the vortex circulation decays from environmental influences;
- Crosswind shear may further reduce the sink rate and in some cases cause a wake vortex to rise;
- Ambient turbulence influences the time of vortex pair linking; i.e. the time of occurrence of crude vortex rings that are elongated along the flight path.

2.2 History of Wake Vortex Research at Langley

NASA Langley has had a long history of conducting wake vortex research. Research areas include wake vortex alleviation, characterization, hazard analysis, and aircraft separation standards. Much of this research is summarized in Chambers¹⁵. Recent programs include developing and demonstrating a concept to increase airport capacity by safely decreasing aircraft separations.^{16,17,18,19} A key element of these programs is to predict the transport and decay of wake vortices in an operational airport environment.^{20,21}

3.0 Analysis of Ambient Conditions

Vertical profiles of the atmospheric wind, temperature, and turbulence intensity are needed to determine the drift and decay of the wake vortices generated during this accident. Also such profiles could indicate unusually vertical wind shears, atmospheric layers, and temperature inversions, as well as give clues to unusual weather phenomenology. Several sources of profiles were examined, but thought unrepresentative. A National Weather Service (NWS) rawinsonde sounding observed at 1200 UTC, from Upton, NY, was thought too old to be representative of conditions at the time of the accident; while data from the ITWS is too coarse in vertical resolution for our specific needs. Therefore, wind and temperature profiles are derived from the FDR of both JAL 47 and AA 587. This data was extracted by NTSB and their analysis is described in the Group Chairman's factual report¹. Vertical wind and temperature profiles are extracted from measurements along the flight path assuming horizontal variations are negligible. Other data sources, including ITWS and weather forecast models, support this assumption since they indicate little or no horizontal variation above the atmospheric boundary layer at the time

and location of the accident. The atmospheric data derived from JAL 47 is preferred since data from AA 587 may have been contaminated by the wake of JAL 47. Also the vertical profile from AA 587 is limited in altitude compared to JAL 47.

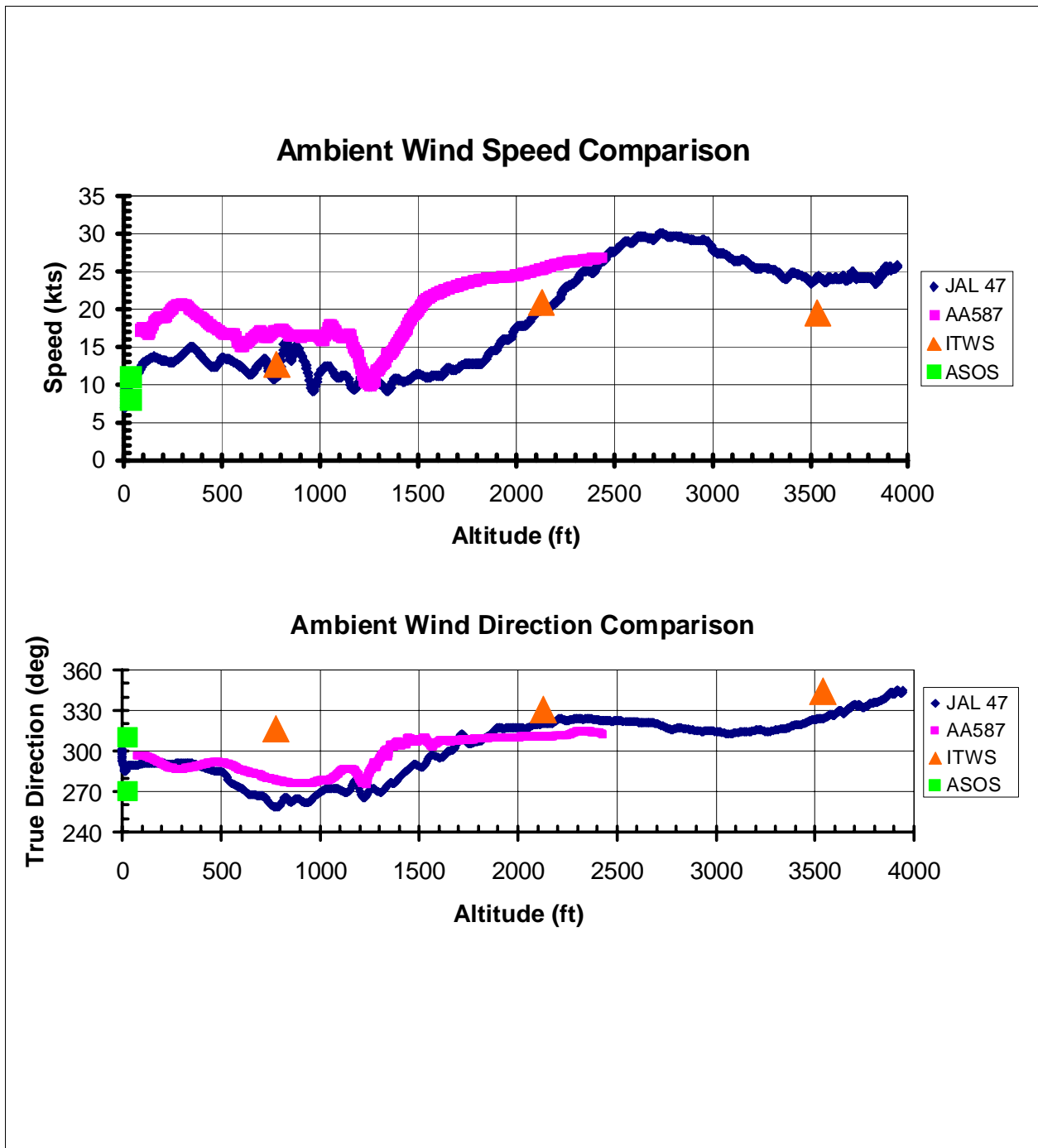


Figure 3. Comparison of measurements for atmospheric wind speed and direction at time of accident (source NTSB¹).

3.1 Ambient Wind Profiles

A comparison of the environmental wind profiles from the FDR's of both aircraft (fig 3) show unexplainable differences. At altitudes below 2400 *ft* (730 *m*) the wind speeds from AA 587 are noticeably stronger than for either JAL 47, ITWS, or ground sensor measurements (ASOS). The differences are suspected to be due to errors and approximations, rather than from real variations experienced between the two aircraft. Wind estimates from aircraft FDR are subject to errors due to accelerations and maneuvers experienced during departure. The JAL 47 winds are thought more reasonable since they better match other independent measurements. Differences between the two FDR profiles are greatest near the altitude of the first suspected wake encounter (1750 *ft*), but least near the altitude of the second encounter (~2430 *ft*). As also shown in fig 3, the profiles for wind direction derived from the two aircraft are mostly consistent.

3.2 Ambient Temperature Profile

The temperature data from JAL 47 (fig 4) does not exhibit any unusual or striking qualities. The temperature profile indicates near neutral stratification up to an altitude of about 1300 *ft* (400 *m*). A small inversion, signifying the top of the atmospheric boundary layer, exists between 1300 and 1525 *ft* (400-465 *m*). Above this altitude the profile is weakly stable, and exhibits an average lapse rate of about $0.0071^{\circ}\text{C m}^{-1}$. The equivalent Brunt-Vaisala frequency for this layer is $N = 8.77 \times 10^{-3} \text{ s}^{-1}$.

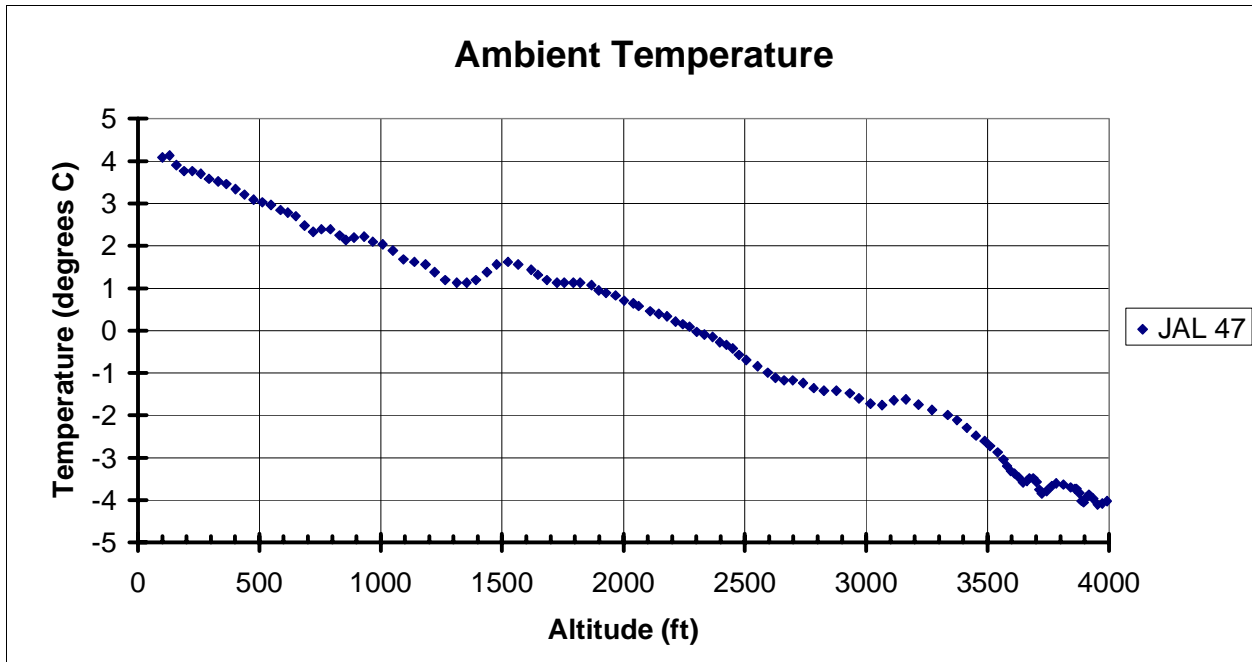


Figure 4. Ambient atmospheric temperature vs altitude from JAL 47.

3.3 Analysis of Wind Profiles from JAL 47

Since the suspected wake encounters occurred at 535 *m* and 745 *m* (1750 - 2450 *ft*) elevation, focus will be on the profiles in this region.

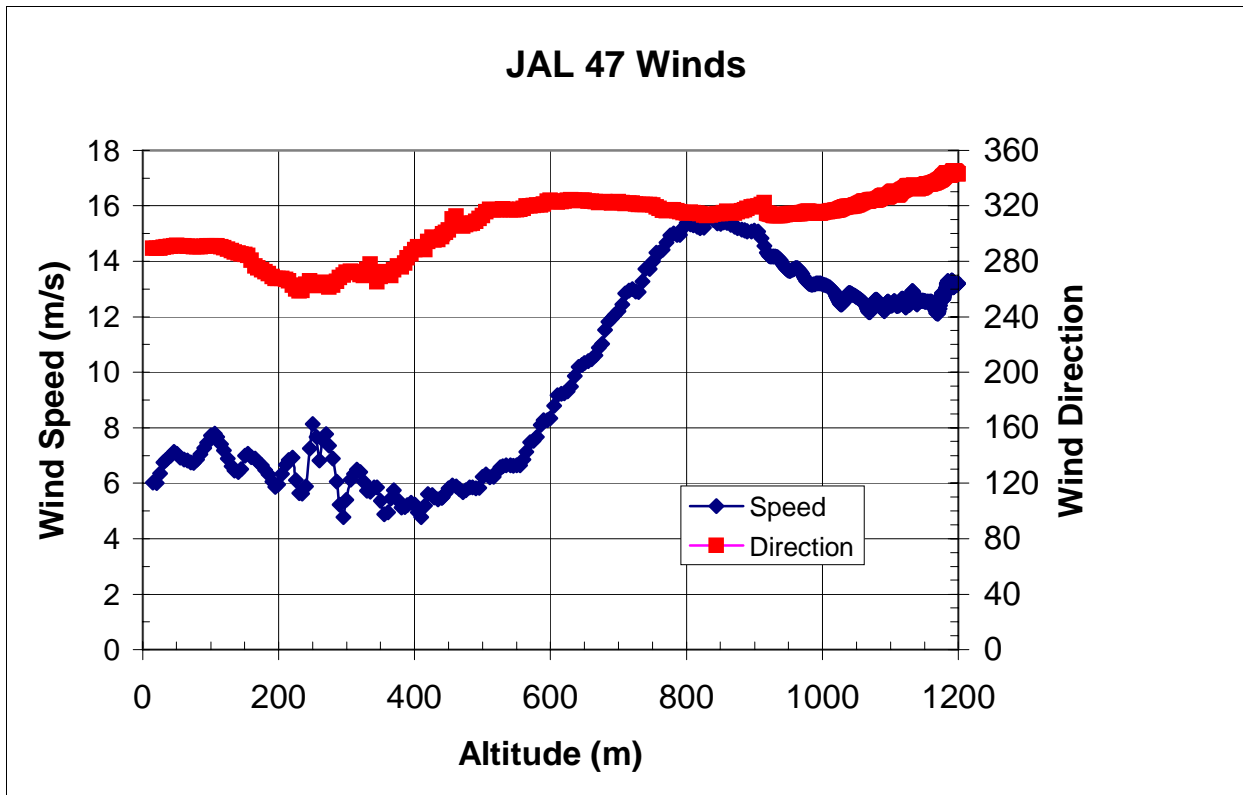


Figure 5. Wind profile from JAL 47.

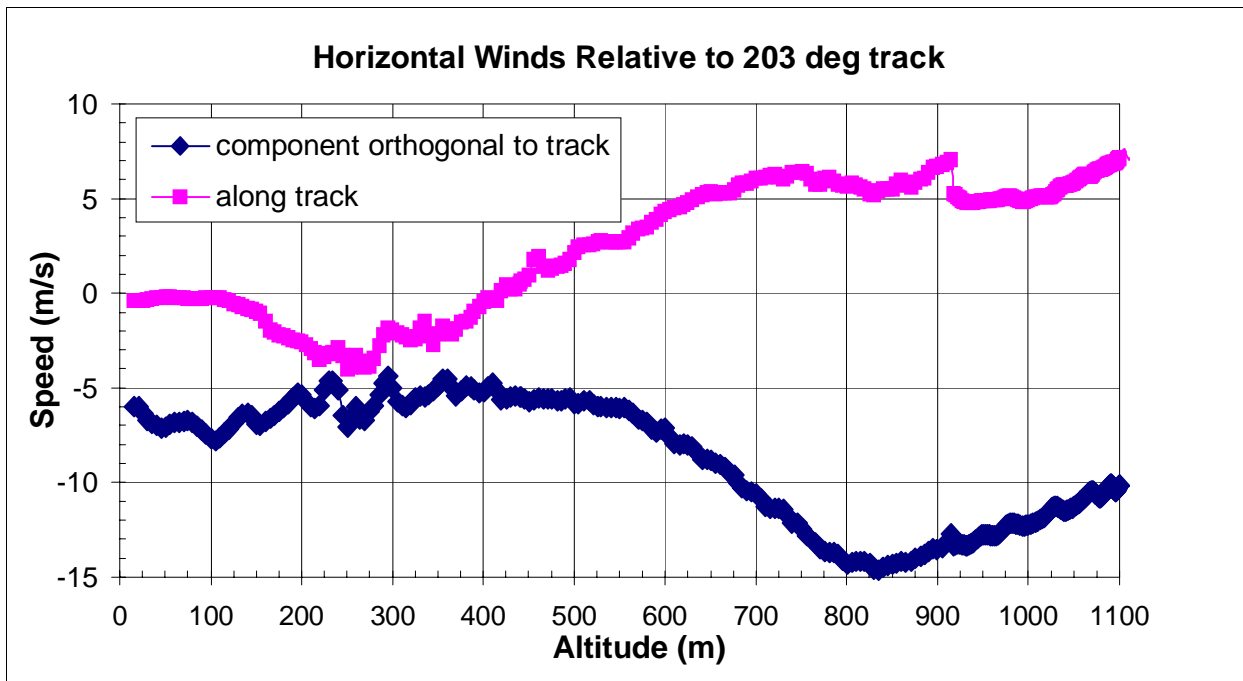


Figure 6. Same as fig 5, but wind components relative to the 203 degree heading of AA 587. Crosswind component is denoted by blue curve.

Figure 5 shows the ambient wind profile from JAL 47. It indicates a nearly constant wind speed in the atmospheric boundary layer of about 6 m/s. Above the boundary layer top (400 m) the wind speed gradually increases with height reaching a peak of over 15 m/s at 850 m elevation.

Figure 6 shows these winds in components relative to a 203° aircraft heading. This value is close to the heading of AA 587 during all of its suspected vortex encounters. Note that there are no unusual variations in the along-track component of wind. The cross-track wind component increases from 5 m/s to 15 m/s between 500 m and 850 m altitude.

In fig 7, the vertical derivative, as well as its second derivative, are computed from the crosswind component shown in fig 6. The magnitudes of crosswind shear are weak in the regions of suspected vortex encounter with values less than $\sim 20 \times 10^{-3} \text{ s}^{-1}$. The second derivative is included since it may affect wake vortex descent.^{20,22} Peak magnitudes for the vertical derivative of shear are about $40 \times 10^{-5} \text{ m}^{-1} \text{ s}^{-1}$. This magnitude of vertical derivative of shear could cause some tilting of the vortex pair with the port vortex being higher in elevation than the starboard.

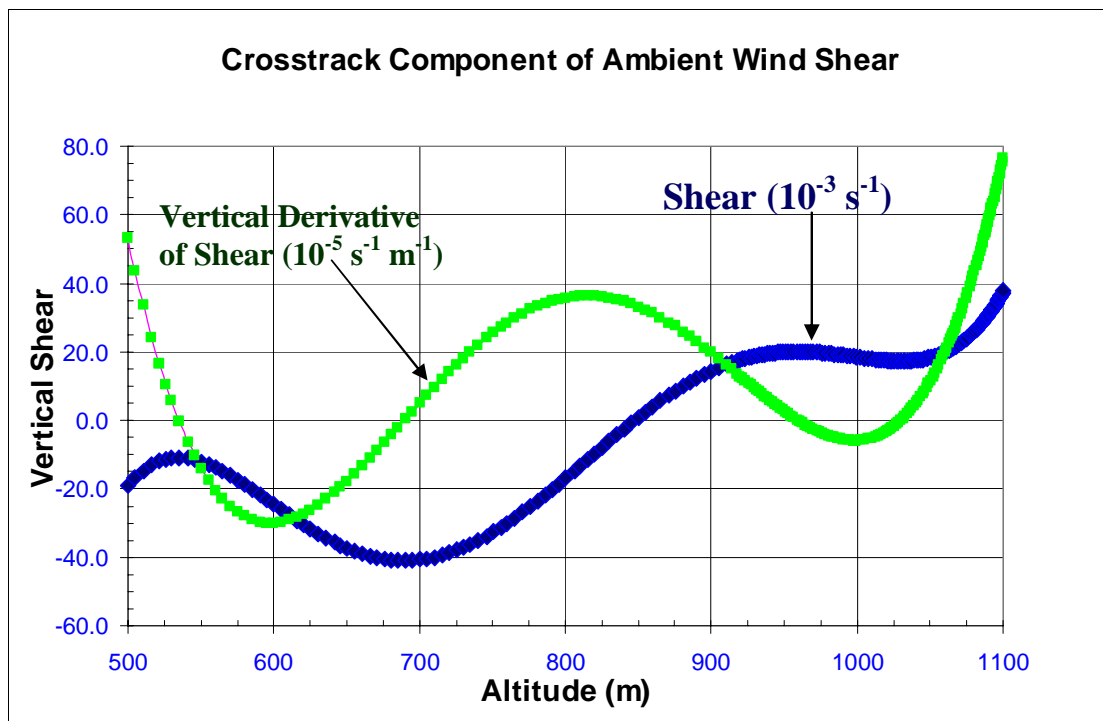


Figure 7. Vertical shear of the crosswind component (blue curve). The second derivative of the crosswind is shown by the blue curve.

3.4 Analysis of Environmental Turbulence

In order to predict the rate of vortex decay for this case, a representative profile of turbulence intensity is needed. To satisfy this requirement, the turbulence eddy dissipation rate (EDR) was estimated from the JAL 47 data by Dr. Roland Bowles, Mr. Paul Robinson and Mr. Bill Buck of AeroTech Research. A vertical profile for EDR (fig 8) was computed from a 5-second window of the vertical accelerations available from JAL 47 FDR. This profile was obtained by assuming

typical response curves for a B-747 following takeoff. Similar techniques for generating EDR profiles from aircraft FDR are described in Buck and Velotas.²³

The profile for turbulence intensity (fig 8) does not show any level of turbulence that would be unusual for a clear day in November. The profile below 400 m (1310 ft) indicates light turbulence with values typical for an atmospheric boundary layer. Above the atmospheric boundary layer (elevations greater than 400 m), the magnitude of turbulence quickly diminishes to very weak intensities. Between altitudes of 535-900 m (1750-2950 ft), specific values for ϵ range between $2 \times 10^{-6} m^2 s^{-3}$ to $5 \times 10^{-5} m^2 s^{-3}$ with an average of about $2.5 \times 10^{-5} m^2 s^{-3}$. These very weak turbulence intensities coupled with modest thermal stratification would imply long lifetimes for wake vortices resident in this layer.

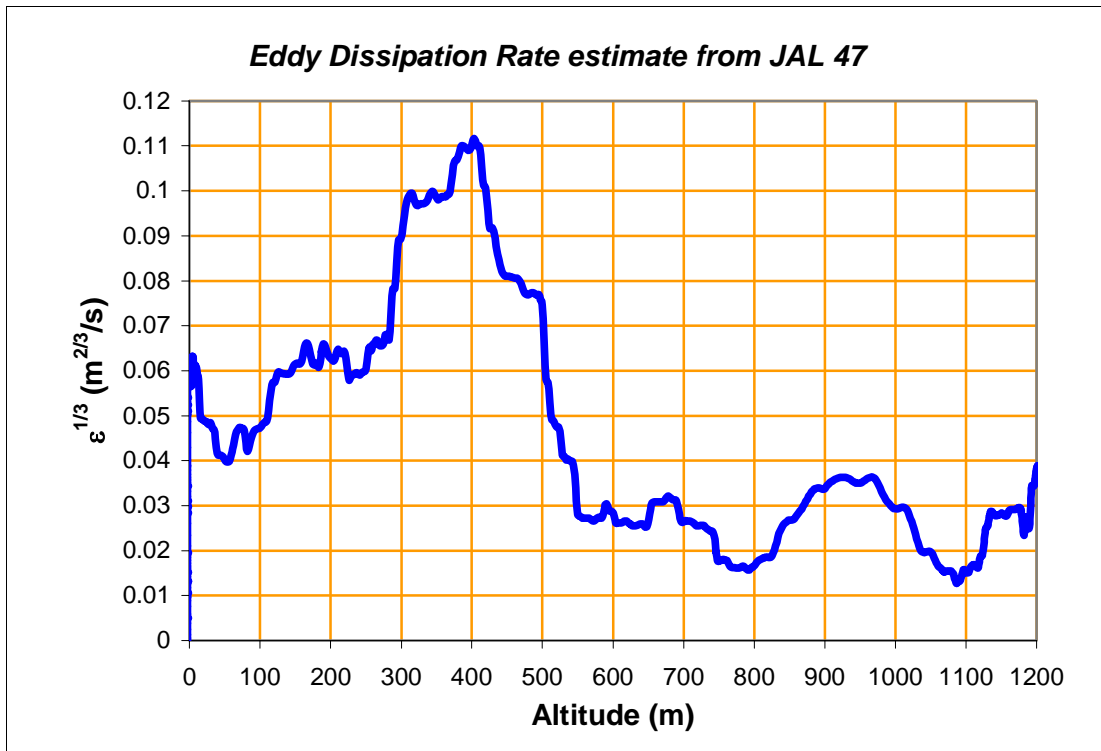


Figure 8. Turbulence eddy dissipation rate as a function of altitude.

4.0 Model Input Parameters

The wake vortices generated by JAL 47 can be analyzed from results of several models. These models need values for input parameters that are representative of the generating aircraft and the ambient conditions near the time and location of the suspected vortex encounters.

4.1 Initial Parameters for Generating Aircraft

In order to generate predictions with our wake vortex models, parameters are needed for initializing the wake strength. The JAL 47 had a gross weight of 780,000 lbs, a wingspan (B) of

64.3 m, and a total mass (M) of 353,802 kg. The airspeed (V_a) and air density (ρ) at altitudes near the suspected wake encounters were 207 knots (106 m/s) and 1.19 kg m^{-3} , respectively. Hence:

$$\begin{aligned} \text{Initial vortex separation:} & \quad b_o = 50.5 \text{ m}; \\ \text{Initial vortex strength:} & \quad \Gamma_\infty = 545 \text{ m}^2 \text{ s}^{-1}; \\ \text{Initial vortex descent speed:} & \quad V_o = \Gamma_\infty / 2\pi b_o = 1.72 \text{ m/s}, \end{aligned}$$

which are determined from conventional formula assuming elliptical wing loading; i.e., $b_o = \pi B/4$, and $\Gamma_\infty = 4Mg/(\pi B\rho V_a)$.

4.2 Environmental Parameters

Constant values for turbulence intensity and thermal stratification are taken from figs 4 and 8, and represent mean values between elevations of 535 - 900 m.

$$\begin{aligned} \text{Ambient thermal stratification:} & \quad N = 8.77 \times 10^{-3} \text{ s}^{-1}; \\ \text{Ambient eddy dissipation rate:} & \quad \varepsilon = 2.5 \times 10^{-5} \text{ m}^2 \text{ s}^{-3}; \end{aligned}$$

Or in nondimension terms:

$$\begin{aligned} \text{Nondimensional Brunt-Vaisala frequency:} & \quad N^* = N b_o / V_o = 0.257 \\ \text{Nondimensional Eddy Dissipation Rate:} & \quad \varepsilon^* = (\varepsilon b_o)^{1/3} / V_o = 0.065 \end{aligned}$$

5.0 Model Predictions for Wake Vortex Strength and Drift

Several different models are used to assess what hazard the wake from JAL 47 might have posed to AA 587. The models are the AVOSS Prediction Algorithm (APA), Terminal Area Simulation System (TASS), and the TASS Driven Algorithms for Wake Prediction (TDAWP). These models and their application to this problem will be described below.

5.1 APA Predictions

The APA model was developed during NASA's Aircraft Vortex Spacing System (AVOSS) project and demonstrated in operational airport environments.^{21,24} APA is a semi-empirical, real-time engineering model for predicting wake vortex transport and decay. The model has theoretical underpinnings and is fine-tuned to data observed during field studies. It computes wake vortex trajectories and circulation decay in a plane perpendicular to the path of the generating aircraft. The algorithm is based on the following assumptions:

- away from the ground, the vortices are transported laterally at the speed of the local crosswind;
- crosswind shear effects are not included, except as might arise from the previous assumption;
- transport due to large-scale turbulence is not included;
- does not account for meandering due to vortex instabilities;
- each member of the wake vortex pair sinks and decays at the same rate;
- the circulation decay rate is independent of vortex radius;
- does not predict the wake vortex wind field distribution;

- accepts as input vertical profiles of atmospheric wind, temperature, and turbulence, as well as physical parameters of the generating aircraft.

Evaluation of the APA model with actual wake measurements is presented in Sarpkaya *et al*²¹ and Robins and Delisi.²⁵

5.1.1 Initialization

The APA model is initialized with the appropriate physical aircraft parameters and environmental profiles for temperature, and turbulence as described in section 4.0. Input profiles for ambient winds are functions of altitude assuming the JAL 47 wind profile (figs 3, 5 and 6). A second set of experiments assume the AA 587 wind profile (see fig 3), and therefore, are limited to examining regions near the first suspected wake encounter. [Wake vortices that might affect the AA 587 in the second wake-encounter region require knowledge of winds at altitudes above AA 587's maximum altitude.]

5.1.2 Approach

The aim of the analysis is to create a four-dimensional view that includes the JAL 47 wake vortices and the paths from both aircraft. The analysis is based on wake vortex predictions with APA, given the altitude and position as a function of time for each aircraft. Two sets of simulations are generated based on the ambient wind profile from the FDR of either AA 587 or JAL 47. In each set of simulations, nine points are chosen along the AA 587 flight path, including two points where wake vortex encounters are suspected. Through each point, two-dimensional planes are constructed that are orthogonal to the JAL 47 flight path. Within each plane, the altitude of the generating aircraft, z_i , and the time difference between the two aircraft, Δt_i are determined from flight data. The position and strength of the wake vortex then is predicted for the time interval, Δt_i within each cross-section. The predicted wake vortex mappings relative to the two aircraft are constructed from the nine simulations in each set. The maps are then animated in time to establish the predicted time of encounter and wake vortex orientation.

5.1.3 Suspected First-Encounter Region

A mapping of the wake vortices from JAL 47 at the time of the suspected first encounter is shown in figs 9-10. For the JAL 47 ambient wind profile, the APA predictions show the wake vortices to have descended to the same altitude as AA 587, but are $\sim 250\text{ m}$ (820 ft) to the west of the aircraft. However, if ambient winds from the AA 587 are assumed, the wind speeds are sufficiently strong to transport the wake vortices into close proximity of AA 587. In this case, a vortex encounter would have occurred from the starboard (right) side of the aircraft. The predicted circulation of the wake vortex is $\sim 345\text{ m}^2\text{s}^{-1}$ or about 63% of initial strength.

From the ambient wind profiles of the two aircraft, it is not conclusive that the first suspected wake encounter was due to the JAL 47 wake. However, this first event seems less important to the accident than the next suspected encounter (other than possibly adding apprehension to the pilots.)

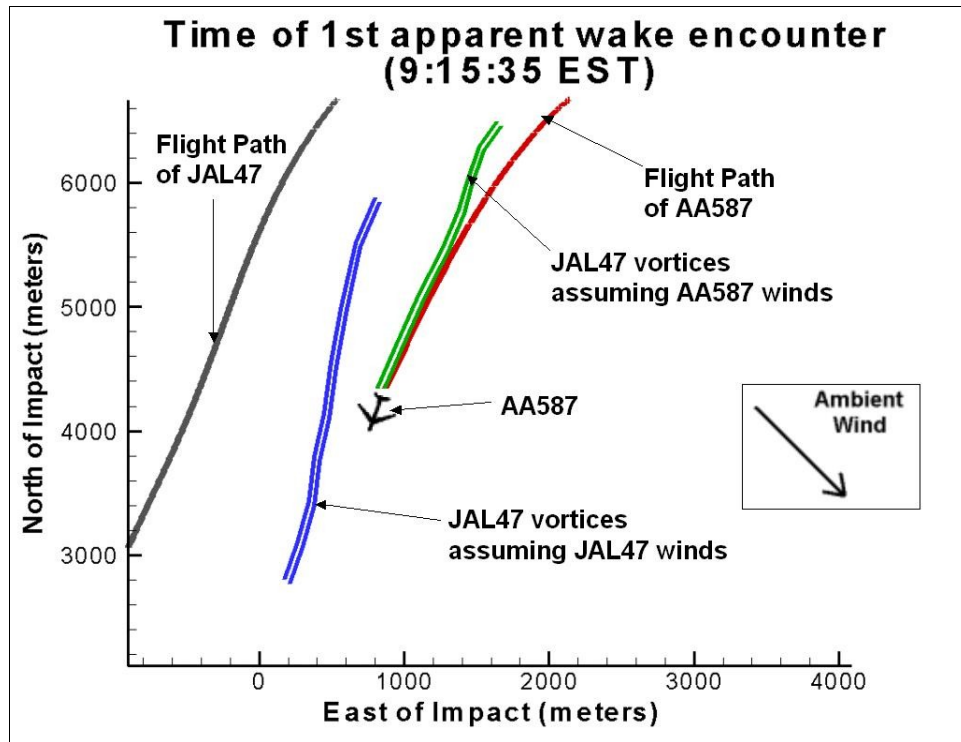


Figure 9. Plan view of aircraft trajectories and wake vortex positions at time of first suspected wake encounter.

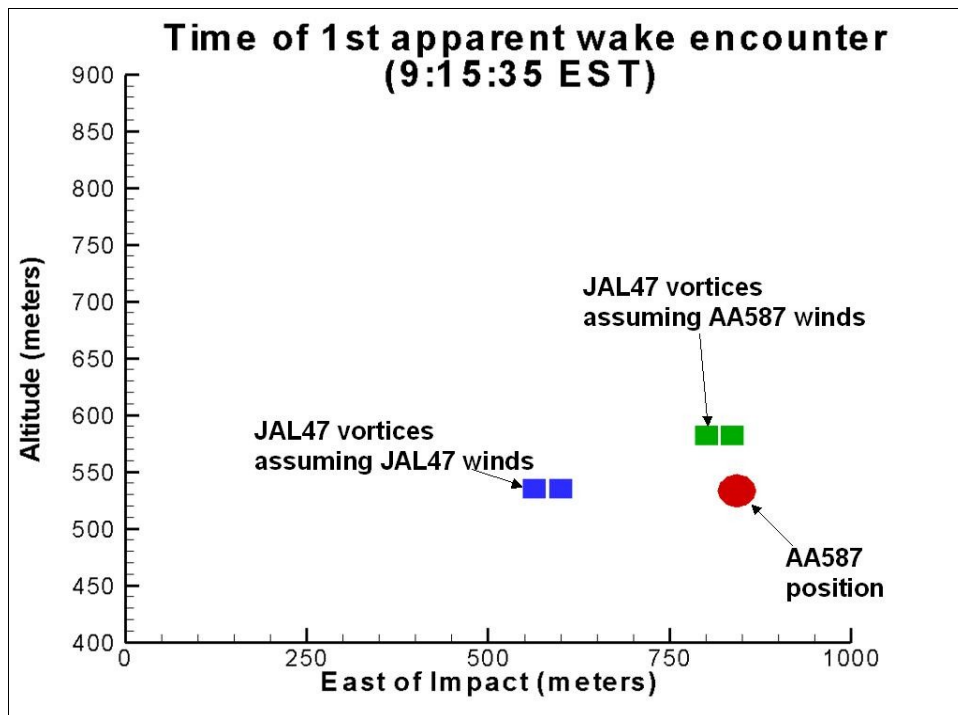


Figure 10. Vertical cross section at location of AA 587 at time of first apparent wake encounter (viewed from south).

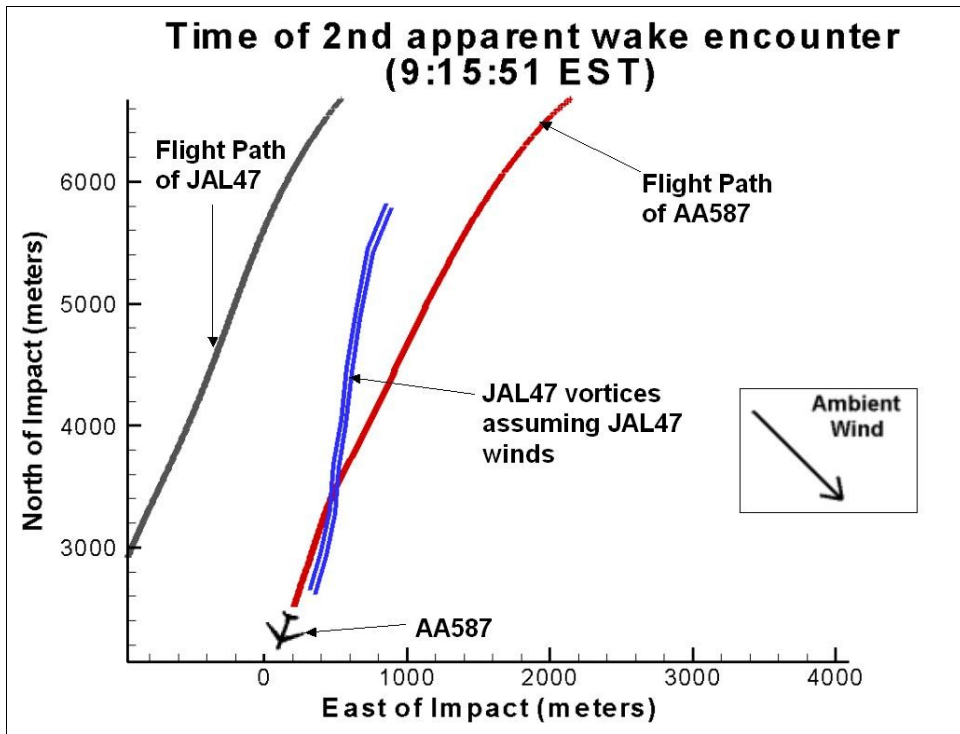


Figure 11. Same as fig 9, but at time of second apparent wake encounter.

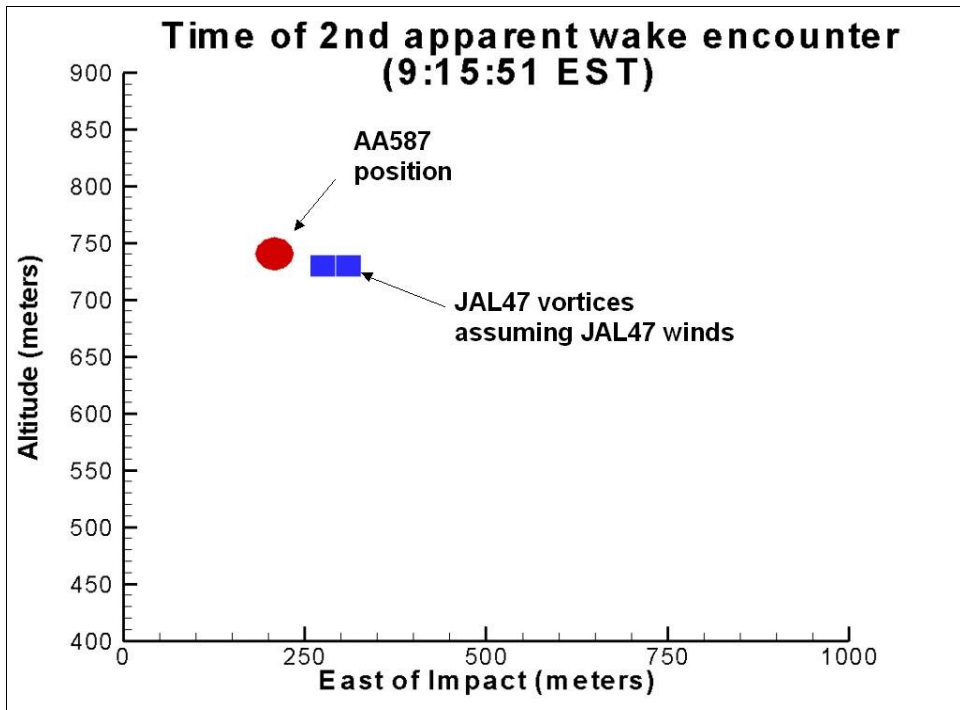


Figure 12. Same as fig 10, but at time of second apparent wake encounter.

5.1.4 Suspected Second-Encounter Region

A mapping of JAL 47's wake vortices at the time of the suspected second encounter is shown in figs 11-12. The APA predictions show the wake vortex to be in close proximity to the AA 587. The age of the wake vortices at the location of the second encounter is about 100 *sec*, or in nondimension time units, $T = t V_o / b_o = 3.4$. The predicted circulation is $345 \text{ m}^2\text{s}^{-1}$ or about 63% of initial strength. The APA predictions indicate that the wake vortices lay on the port side of AA 587, with the aircraft trajectory being nearly parallel to the axis of the wake vortices. Hence, the APA predictions support a sustained encounter with a strong wake vortex within the region of the suspected second encounter.

5.2 TDAWP Predictions

The TASS Driven Algorithms for Wake Prediction (TDAWP) is a simple set of algorithms engineered from results of three-dimensional large eddy simulations of wake vortices. The model consists of two equations, one for the prediction of vortex transport and a second for wake vortex decay. This model predicts somewhat different values than APA and is incorporated here for comparison. Predictions for TDAWP are computed only for the second encounter region. Neither APA nor TDAWP include the effects of ambient wind shear on vortex sink rate and decay. A detailed description of TDAWP, including validation with field data, is included in the appendix A.

The decay of circulation and vortex descent are predicted for the wake generated by JAL 47 assuming the parameters in section 4. Like APA, TDAWP predicts a relatively long-lasting vortex due to the low intensity of background turbulence and the moderate level of thermal stratification. At the time of the wake encounter ($t = 100 \text{ s}$), TDAWP predicts a 10-15 *m* average circulation of $397 \text{ m}^2\text{s}^{-1}$ and a vortex descent of 160 *m* (525 *ft*). Hence, TDAWP predicts a wake vortex that is about 15% stronger and that descends an additional 20 *m* (66 *ft*) than predicted with APA. TDAWP, like APA, supports an encounter with a strong wake vortex prior to the crash off AA 587.

5.3 Three-Dimensional TASS Predictions

Two- and three-dimensional wind field distributions are needed in order to conduct aircraft simulator studies and better understand how the aircraft and pilot may have responded to the wake vortex encounter. Also, such wind field models can be beneficial in modifying aircraft and teaching pilots to better respond if caught in a similar hazard. The previously discussed APA and TDAWP models are valuable in determining whether the wake vortex from JAL 47 could have drifted into the path of AA 587, but these models do not predict vortex wind field distributions. Three-dimensional wind fields representing the wake vortex generated by JAL 47 and encountered by AA 587, can be produced by a three-dimensional, large-eddy simulation (LES) model called the Terminal Area Simulation System (TASS)^{22,26}. Salient features of TASS are listed in Table 1. A brief description of TASS is given in appendix B.

The TASS model has been applied in a recent NASA wake vortex program, and was used to investigate how aircraft trailing vortices interact with the atmosphere. In previous wake vortex studies, TASS has demonstrated good agreement with observational data.^{20,22,27,28,29}

Computations with the three-dimensional version of TASS require state-of-the-art supercomputers in order to achieve both adequate resolution and sufficient domain size; and therefore, cannot be used in an operational setting as the more simplified engineering models such as APA and TDAWP. Here, the primary application of TASS is to generate detailed wind fields representing the wake vortex from JAL 47.

Initializing TASS with conditions representing those observed during the accident can generate wind fields similar to those encountered by AA 587. The approach used here is similar to that of previous wake vortex investigations with TASS.

Table 1. Salient Characteristics of TASS.

- Time-dependent, nonhydrostatic, compressible, nonBoussinesq, primitive equation set.
- Meteorological framework with option for either three-dimensional or two-dimensional simulations.
- Large Eddy Simulation model with subgrid-scale turbulence closure – Grid-scale turbulence explicitly computed, while effects of subgrid-scale turbulence modeled by Smagorinsky model with modifications for stratification and flow rotation.
- Optional conditions for lateral, top, and ground boundaries.
- Explicit numerical schemes, quadratic conservative, time-split compressible—accurate, highly efficient, and essentially free of numerical diffusion. Space derivatives computed on Arakawa C-grid staggered mesh with 4th-order accuracy for convective terms.
- Prognostic equations for vapor and atmospheric water substance (e.g. cloud droplets, rain, snow, hail, ice crystals). Large set of microphysical-parameterization models.
- Model applicable to meso- γ and microscale atmospheric phenomenon. Initialization modules for simulation of convective storms, microbursts, atmospheric boundary layer turbulence, convectively induced turbulence, and aircraft wake vortices.
- Accepts vertical profiles of environmental temperature, moisture and winds as input.
- Output includes time-dependent, three-dimensional fields for atmospheric winds, temperature, pressure, and moisture.

5.3.1 Model Domain

The model domain has an x , y , z coordinate system with the x -coordinate in the direction of the generating aircraft (along track), y , the lateral coordinate (cross track), and z , the vertical coordinate. Similarly, u represents the wind component in the along-track direction, v is the crosswind component, and w is the vertical wind component. Since the accident occurs well above any ground effect, the influence of the ground is not modeled and periodic conditions are assumed on all boundaries. The number of grid points in the x , y , z directions are 481, 433, and 241, respectively; resulting in over 50 million grid points per variable and time step. The grid spacing is 2 m in the x direction, and 1.5 m in the y and z directions. Starting with the initial conditions, a time integration for 100 seconds is performed, arriving at a solution representing the JAL 47 wake vortex field at the time of the AA 587 encounter.

5.3.1 Initialization Parameters

The TASS model is initialized with the appropriate physical aircraft parameters and environmental profiles for temperature and turbulence as described in section 4.0. For simplicity, environmental wind shear is not included in this calculation.

The wake vortices are initiated at an altitude of 883 m. Specifics of the wake vortex and turbulence initiation are below.

5.3.1.1 Turbulence initiation

Prior to vortex initialization, an environmental field of resolved-scale turbulence is allowed to develop under an artificial external forcing at low wavenumbers.³⁰ The turbulence field has a Kolmogorov³¹ spectrum with an eddy dissipation rate of $\varepsilon = 2.5 \times 10^{-5} \text{ m}^2\text{s}^{-3}$. This approach is identical to that used in recent studies with TASS, where wake vortex decay and the development of Crow instability is examined within a field of homogeneous turbulence.^{26, 28, 32}

5.3.1.2 Wake vortex initiation

As in previous TASS simulations of wake vortices, a simple vortex system is assumed that is representative of the post roll-up, wake-vortex velocity field of the generating aircraft. The vortex system is initialized with the superposition of two counter-rotating vortices that have no initial variation in the axial direction and are separated laterally by a distance, b_o . The tangential velocity, V , associated with each vortex, is determined from:

$$V(r) = \frac{\Gamma_\infty}{2\pi r} \left[1 - \text{Exp} \left\{ -10 \left(\frac{r}{B} \right)^{0.75} \right\} \right] \quad \text{for } r > 1.4 r_c$$

where, r is the radius from the center of a vortex, and r_c is the core radius. The model is applied only at $r > 1.4 r_c$ and is matched with a Lamb-Oseen model³³ for $r < 1.4 r_c$. Once a suitable turbulence field is generated, the initial wake vortex field is superimposed, assuming a core radius of 3 m and values listed in section 4.0.

5.3.2 Three-Dimensional TASS Results

Figure 13 shows a perspective of the simulated wake vortex at $t = 100 \text{ s}$, or at about the age of the wake vortex during the suspected second encounter. The field is representative of the structure of the wake vortex at distance of $\sim 10.6 \text{ km}$ (5.77 NM) behind JAL 47. Sinusoidal instabilities are beginning to show as a precursor of Crow linking. As is typical for wake vortices undergoing the onset of Crow instability, the vortex separation is most narrow at its lowest point and greatest at its highest point. The two counter-rotating vortices will eventually link at the spots where the separation is most narrow, forming crude vortex rings.

Although the linking process is underway at the time and location of the apparent encounters, the simulation indicates that vortex linking does not occur until the vortices have aged an additional 21 seconds. This value for time to link is predicted also with Sarpkaya's³⁴ reformulation of Crow and Bate's³⁵ analytical model (see appendix A).

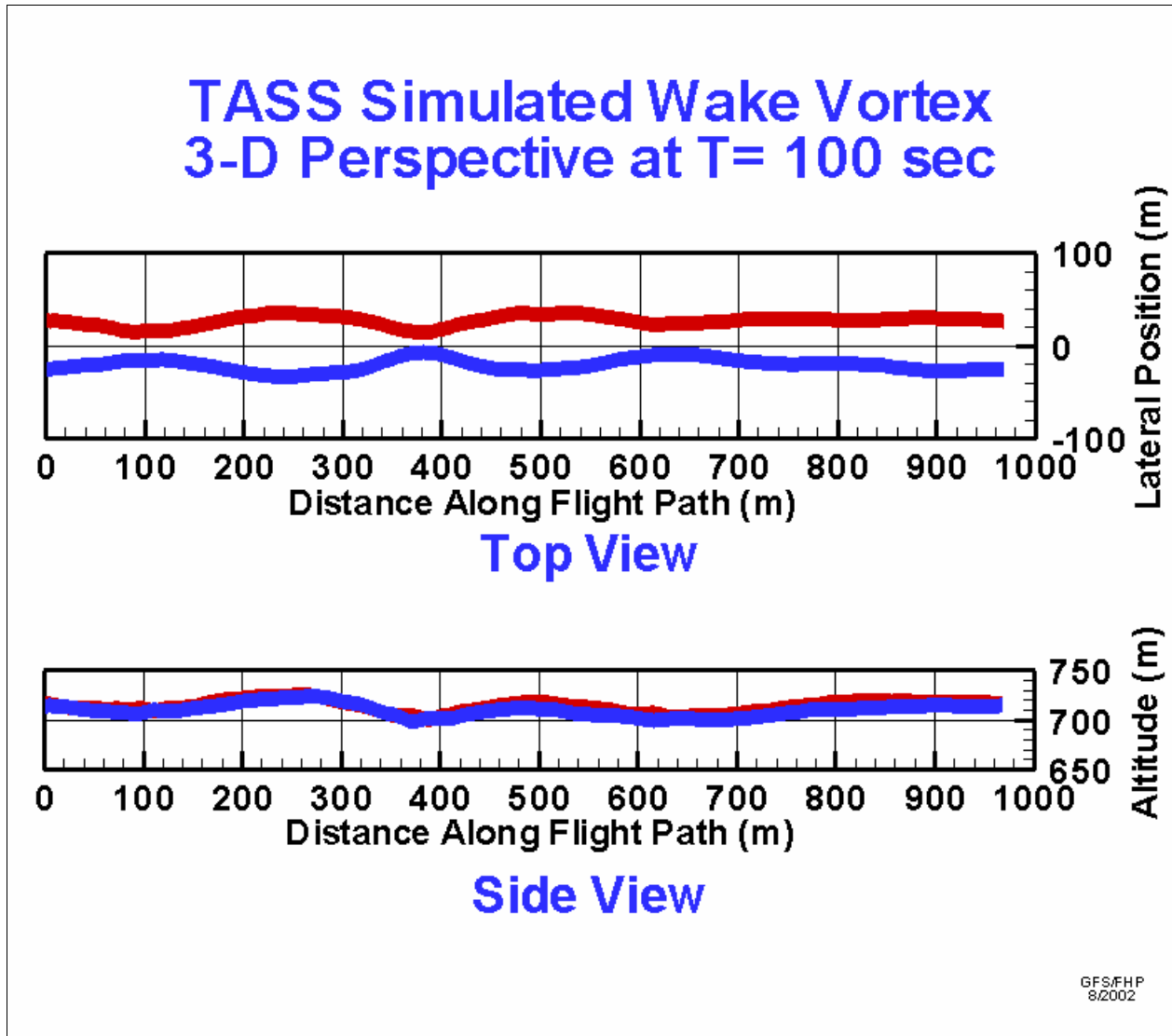


Figure 13. Three-dimensional perspective of simulated JAL 47 wake vortex at time of encounter.

According to Crow's linear instability theory,⁸ the wavelength of wake vortex linking is about $8.6 b_o$; however, the presence of ambient turbulence may shorten this wavelength.³⁶ A recent numerical study by Han *et al*²⁶ shows the most amplified wavelength decreased from $8 b_o$ for very light turbulence to $4 b_o$ for moderate turbulence. In our simulation, the most amplified wavelength of the vortex oscillations is about $260 m$ or $5.2 b_o$. This is smaller than that predicted from linear instability theory; but is consistent with Han *et al*.

In the time prior to vortex linking the modeled wake vortices decay slowly. The average $5-15 m$ circulation at 100 seconds was $393 m^2 s^{-1}$, or about 80% of initial strength.

Vertical cross sections that are orthogonal to the vortex at its narrowest and widest separations are shown in figs 14 and 15, respectively. It is obvious that the velocity fields are three-dimensional with velocity fields varying along track, as well as in the lateral and vertical

directions. The onset of linking instability causes obvious variation in the flow field between each cross-sectional plane. The altitude of the vortex 100 seconds after generation varied from 707-733 *m*, giving a vertical descent between 151-176 *m* (495-577 *ft*). The lateral drift within the 100 *s* period varied between 1425-1470 *m* (0.769-0.793 *NM*).

This structure raises the question as to whether a single two-dimensional flow field would be appropriate for simulator studies of this case. Also, could these along track-oscillations have played some role in inducing the accident? This issue will be discussed further in the next section.

6.0 TASS Model Data Sets

From the numerical simulation described in section 5.3, data sets containing wind, temperature, and pressure can be provided for additional studies, such as input into analytical flight simulations and flight simulator evaluations. These data sets assume that the JAL 47 wake vortex has aged ~100 *s*, and represents the flow field at the time encountered by AA 587. Available are:

- fully 3-D data set at $t = 100$ *s*,
very large: 481 x 432 x 241 data points for each of the three velocity components;
- one or more *y-z* cross sections,
432 x 241 data points per cross section for each velocity component;
- simple algebraic model fit to data set.

6.1 Discretized data sets

The full 3-D data sets are discretized on a *x,y,z* coordinated grid as described in section 5.3.1. Data from each variable is interpolated to identical grid intervals and stored on compact disks in ASCII format.

6.2 Simple model fit

A model fit to the average vortex profile is shown in fig 16. The mean profile from TASS is determined by first locating the center of the vortex in each cross sectional plane, computing the tangential velocity relative to the center, then averaging the tangential velocity from each plane. A very good fit to the TASS data at 100 seconds is given by

$$V_{tan}(r) = \frac{\Gamma_{\infty}}{2\pi} \frac{r}{(r^2 + r_c^2)}$$

with $\Gamma_{\infty} = 495$ m^2/s , $r_c = 4.5$ *m*, where *r* is radius from the vortex center. Disadvantages of this model are that only one vortex is represented and it does not include axial (i.e. three-dimensional) variations of the flow.

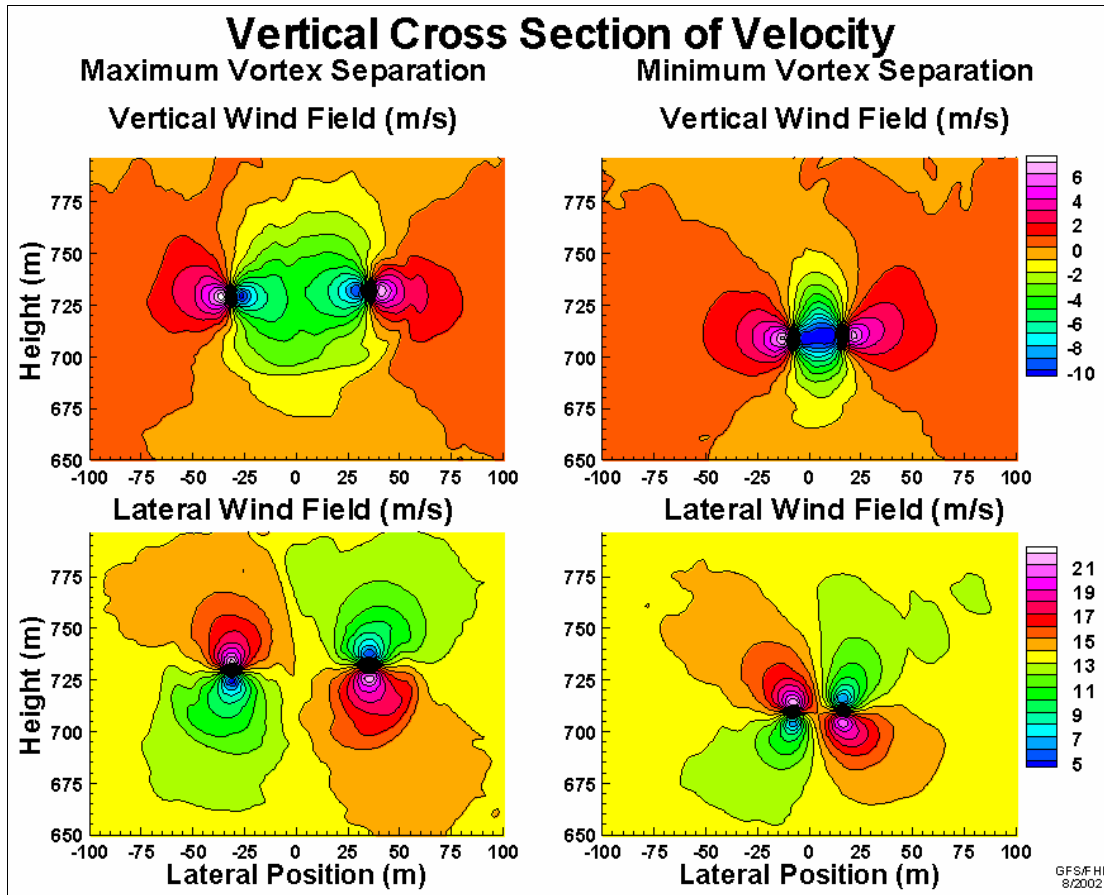


Figure 14. Simulated contour fields of velocity at time of encounter (100 seconds).

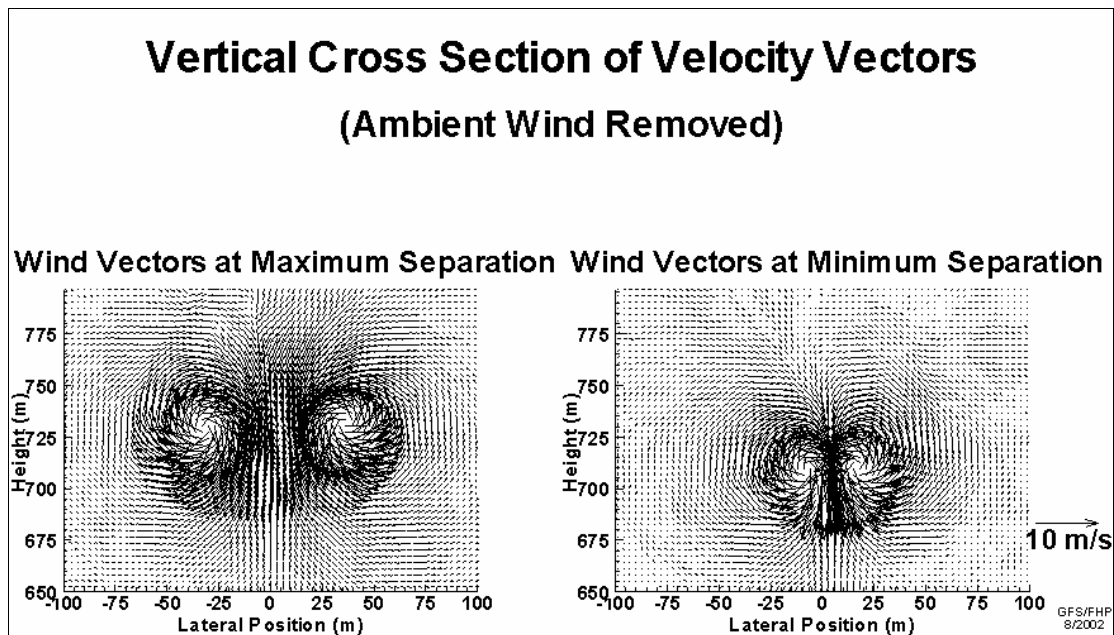


Figure 15. Same as fig 14, but for wind vector field

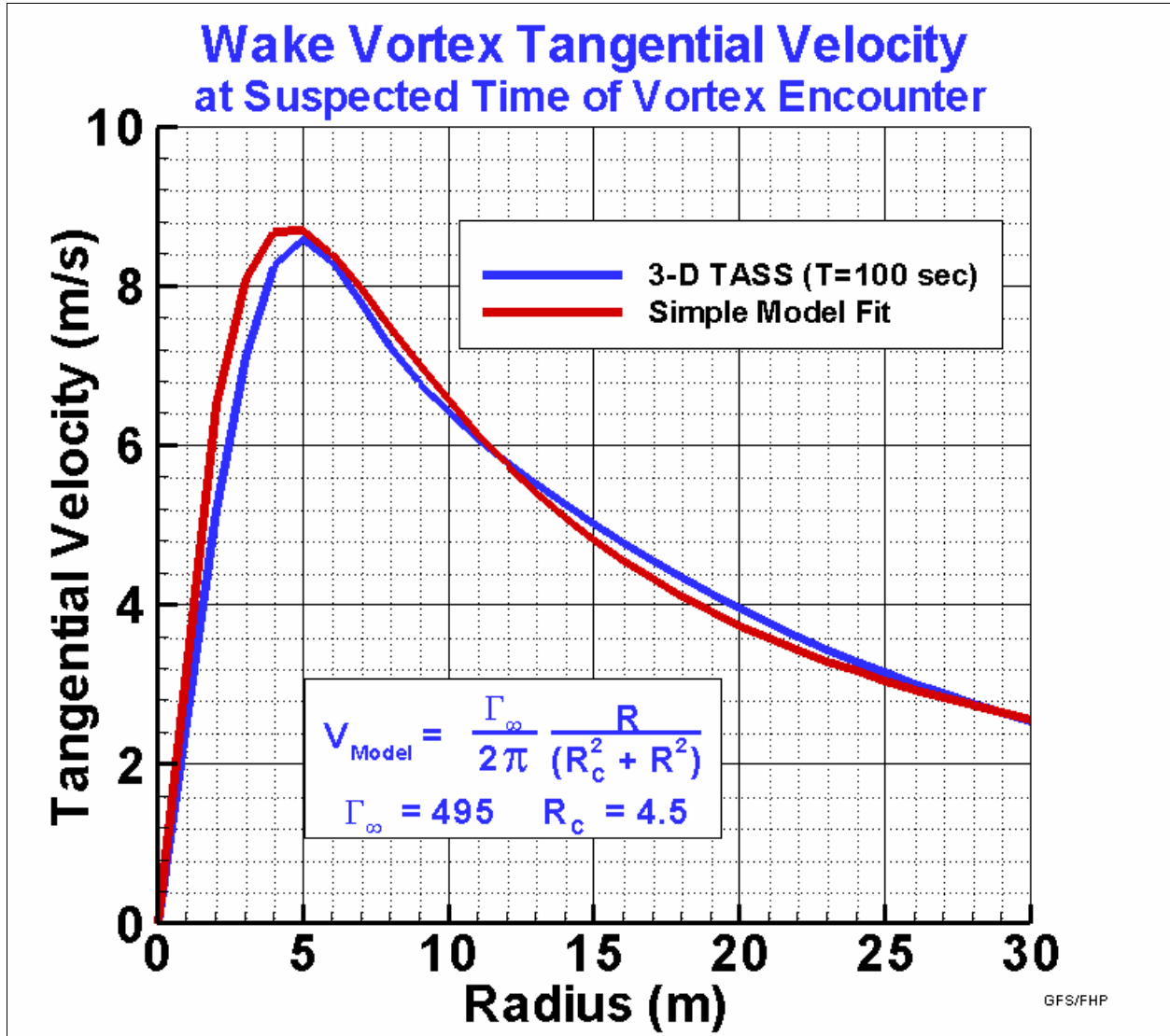


Figure 16. Simple model fit to TASS wake vortex at 100 seconds.

6.3 Algebraic model for wake vortex wind field

As an alternative to a large data set, but with more complexity than a simple vortex model, an algebraic model representing the wake vortex velocity field is provided. The model is based on the output of the TASS 3-D simulation at $t = 100$ s, as described earlier. The model is developed by superimposing two counter-rotating vortices with profiles of tangential velocity based on TASS output. The coordinate system assumed by this model is shown in fig 17, and the equations are expressed below:

Coordinates for Vortex System

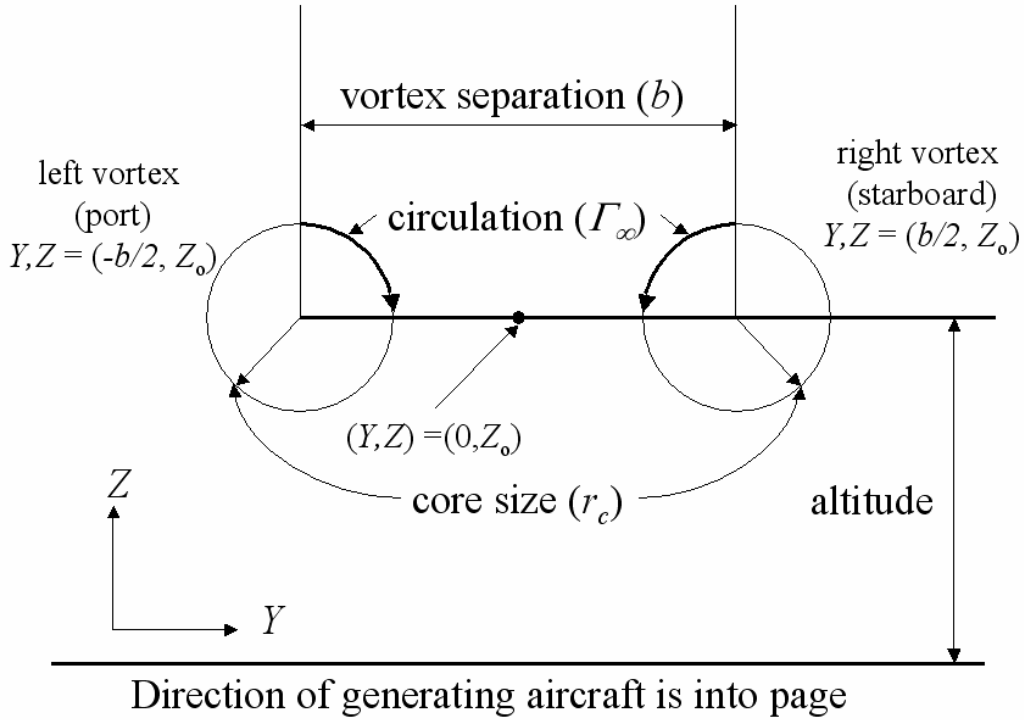


Figure 17. Coordinates for algebraic model fit of AA 587 vortex system.

$$\vec{V}(X, Y, Z) = v\hat{j} + w\hat{k}$$

$$\vec{V} = \left\{ \frac{\Gamma_{\infty}(Z - Z_0)}{2\pi[(Y + b/2)^2 + (Z - Z_0)^2 + r_c^2]} - \frac{\Gamma_{\infty}(Z - Z_0)}{2\pi[(Y - b/2)^2 + (Z - Z_0)^2 + r_c^2]} + v_{\text{ambient}} \right\} \hat{j} + \left\{ \frac{\Gamma_{\infty}(Y - b/2)}{2\pi[(Y - b/2)^2 + (Z - Z_0)^2 + r_c^2]} - \frac{\Gamma_{\infty}(Y + b/2)}{2\pi[(Y + b/2)^2 + (Z - Z_0)^2 + r_c^2]} \right\} \hat{k}$$

where: $Z_0(X) = a_1/2 \sin(2\pi X/\lambda) + C_1 X$,

$b(X) = a_0 + a_1 \sin(2\pi X/\lambda)$,

and with the following constants:

$\Gamma_{\infty} = 495 \text{ m}^2/\text{s}$, $r_c = 4.5 \text{ m}$, $a_0 = 45 \text{ m}$, $a_1 = 22 \text{ m}$, and $\lambda = 260 \text{ m}$.

Note that for a periodic vortex which oscillates vertically about $Z=0$, then $C_I = 0$. This will suffice for most applications. However, if one wishes to add the vertical slope of the vortex pair due to the vortex sink rate and climb rate of the generating aircraft, then:

$$C_I = \{\Gamma_\infty / 2\pi a_0 + dZ/dt)_a\} / V_a$$

where V_a is the airspeed and $dZ/dt)_a$ is the climb rate of the generating aircraft.

The three-dimensionality that is captured by the algebraic model is illustrated in fig 18. The growing sinusoidal oscillations from the onset of crow instability are correctly centered on to planes that are offset 45° from the vertical.

To demonstrate the significance of the along path variation of the flow field, a profile is extrapolated along x at $y=25m$ and $z=5m$, with $C_I = 0$ (fig 19). Note that both the cross flow and vertical velocity change sign with a period of $260 m$. This is due to the effect of the developing crow instability, which causes the vortex to oscillate along a plane slanted 45° degrees from the vertical. If the aircraft were traveling at a speed of $122 m/s$ (as was AA 587), then it would encounter one complete oscillation every $2.1 s$. In other words, the aircraft would encounter an updraft with a crosswind to port, reversing to a downdraft with a crosswind to starboard in about *one second*. Rudder deflections out of sync with this motion might only amplify the loss of stability and control. The above model should be investigated in theoretical and flight simulation studies to determine if a similar scenario may have occurred for AA 587, which experienced opposite changes in rudder inputs about every one second just before the crash.

7.0 Summary and Conclusions

Analysis shows that the flight path of AA 587 was downwind and below the path of JAL 47. Application of wake vortex prediction models, initiated with available environmental data, indicates that the wake vortex from JAL 47 was likely transported into the path AA 587. Atmospheric conditions aloft were favorable for a slow rate of vortex decay; the predicted circulations at the time of the apparent encounter were 63-80% of the initial strength. At the time of the suspected encounter the B-747 wake vortex would have had an age of about 100 seconds, and would have descended about $140-176 m$ ($460-577 ft$). At this age the wake vortex was beginning to develop sinusoidal oscillations resulting from the onset of Crow instability. These oscillations might also have contributed to the accident, but this needs to be investigated further in situation and flight response studies.

Investigation of the weather surrounding JFK shows no atypical weather conditions or phenomenology. In fact, the weather conditions surrounding the accident were fair, with no unusual wind shear, low-turbulence, excellent visibility, and weak stable stratification.

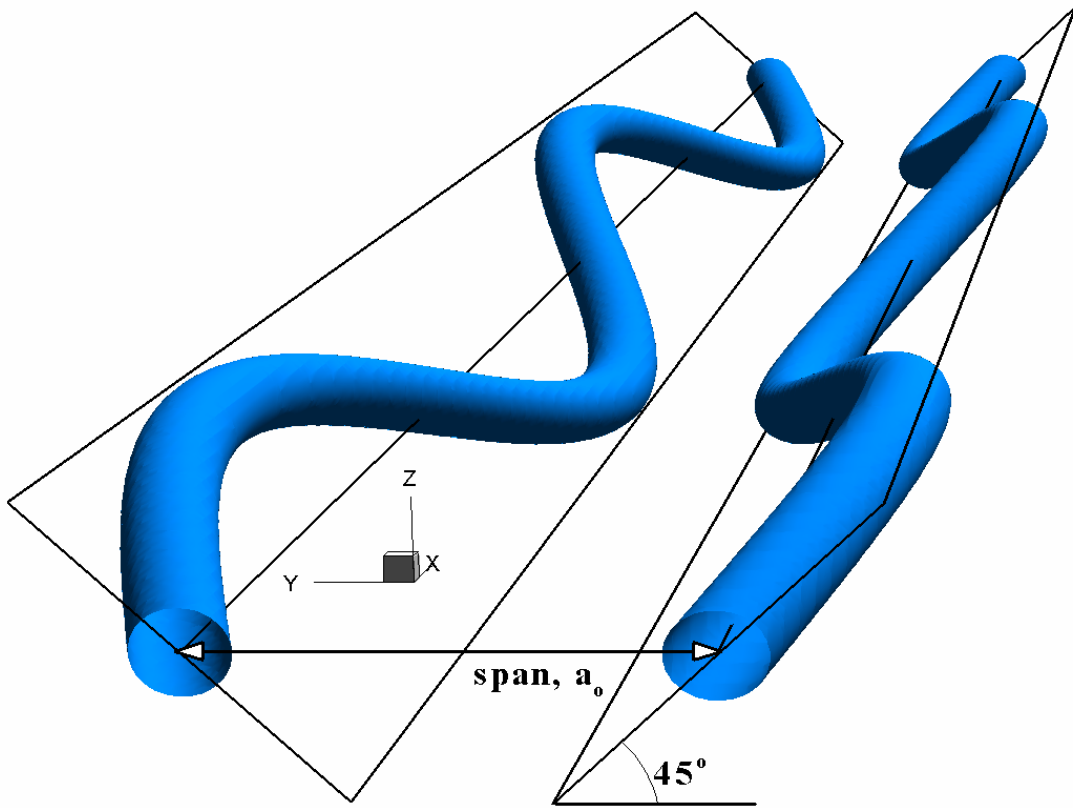


Figure 18. Three-dimensional projection of vortex pair from proposed algebraic model (with $C_1=0$).

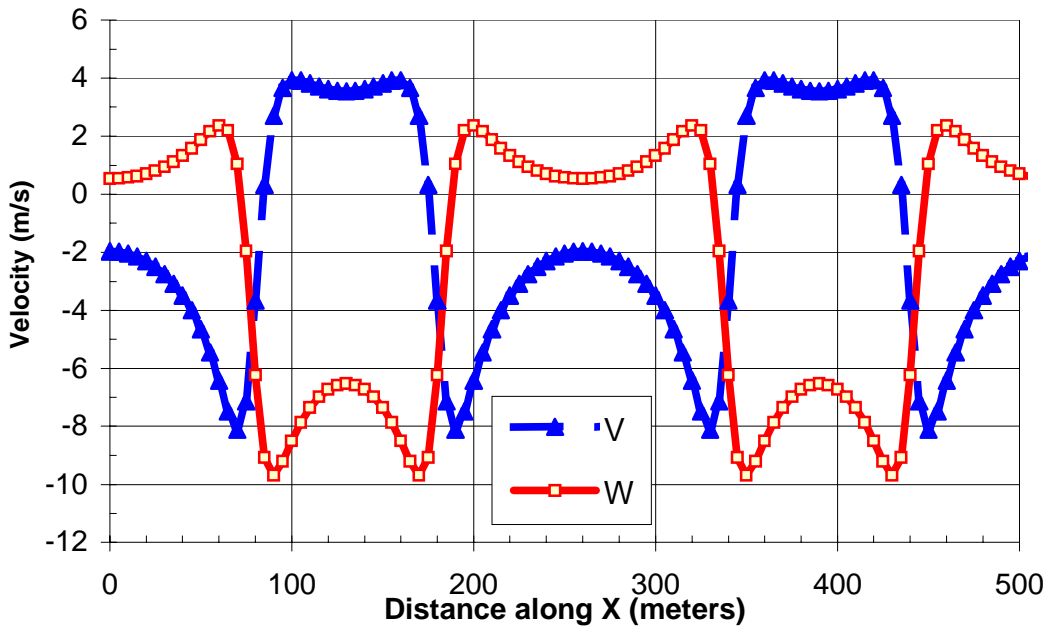


Figure 19. Profile of vertical velocity (w) and lateral velocity (v) along a flight path located at $z=5m$, $y=25m$. Change in velocities due to sinusoidal oscillation of vortex center.

8.0 Acknowledgements

This study was carried out at the request of the National Transportation and Safety Board (NTSB). Atmospheric data and processed flight data was provided by the NTSB. Eddy Dissipation Rate was processed by AeroTech Research from flight data provided by the NTSB. TASS model computations were carried out on the NASA Ames supercomputers. Results from this report were presented in Washington, DC, on 30 October 2002, at the NTSB hearing on American Airline Flight 587.

Appendix-A. TDAWP: TASS Driven Algorithms for Wake Prediction

Nomenclature

A	proportional to cross-sectional area of vortex oval
A_1	constant related to A , $=0.42$
A_2	constant related to A , $=0.035$
B	Wingspan of generating aircraft
b_o	initial vortex separation, $\pi B/4$
c_1	constant, $=0.19$
c_2	constant, $=0.22$
g	acceleration due to gravity, $=9.8 \text{ m s}^{-2}$
N	Brunt-Vaisala frequency, $[(g/\theta) \partial\theta/\partial z]^{0.5}$
N^*	nondimensional Brunt-Vaisala frequency, $2\pi N b_o^2/\Gamma_\infty$
r	radius from vortex center
t	time coordinate ($t=0$ at vortex generation)
T	nondimensional time, $t V_o/b_o$
T_L	nondimensional time to vortex linking
V^*	vortex descent velocity normalized by V_o
V_o	initial vortex descent velocity, $\Gamma_\infty/(2 \pi b_o)$
x	along track coordinate
y	cross track coordinate
z	vertical coordinate
z_o	generating height
Z	nondimensional vertical coordinate, $(z-z_o)/b_o$
Γ^*	normalized vortex circulation at $r=b_o$
$\bar{\Gamma}$	Normalized 10-15 m average circulation
Γ_∞	initial vortex circulation (at $r \gg r_c$)
α_1	constant, $=4/3$
α_2	constant, $=15/8$
β_1	constant, $=3/5$
β_2	constant, $=0.68$
β_3	constant, $=1/4$
γ	constant, $=3/8$
ε	turbulence (eddy) dissipation rate
ε^*	nondimensional ε , $(\varepsilon b_o)^{1/3} V_o^{-1}$
ζ	component of vorticity in direction of flight path
θ	potential temperature
ν	kinematic viscosity, $=1.34 \times 10^{-5} \text{ m}^2 \text{ s}^{-1}$
τ	temperature

Model Concept

The TASS Driven Algorithms for Wake Prediction (TDAWP) is a simple set of algorithms engineered from results of three-dimensional large eddy simulations of wake vortices. The

TDAMP model does not include influence from either ground effect or nonlinear crosswind shear. The model has an advantage over other simple engineering models in that it has separate prediction equations for wake vortex hazard and vortex descent rate, as was originally conceived in Switzer and Proctor³⁷. Vertical variation in N and ε are not considered in the model's present form.

Motivation for the development of TDAMP is provided by results from TASS presented in Switzer and Proctor³². This study showed that stable stratification causes vortex circulation to decay more rapidly at large radii than near the core ($r \leq 15 \text{ m}$). Thus, a unique value for circulation representing both the vortex sink rate and hazard may not be achievable. The nonuniform decay of circulation with radius can become an issue, since the vortex descent rate is influenced by circulation at radii that are comparable to the vortex separation ($\sim b_o$), while the vortex hazard should be evaluated from an average circulation at smaller radii¹³ (i.e. 10 to 15 m radius). Previous vortex prediction models, such as proposed by Greene³⁸, Sarpkaya³⁴, and Holzaephel³⁹, utilize a single prediction equation and assume a uniform circulation which relates to vortex descent as well as hazard.

The proposed model also attempts to capture the sequence of decay phases as simulated in TASS and other LES results. In the first phase of circulation decay, turbulence diffusion dominates. The vortex circulation decays simultaneously at all vortex radii, with the rate of decay being slightly greater at the smaller radii.²⁸ This rate of decay occurs without core growth and in proportion to the intensity of ambient turbulence. This first phase is not to be confused with laminar decay, which weakens the vortex from the inside by growing the diameter of the vortex core. Laminar decay is insignificant within atmospheric wake vortices due to the high rotational Reynolds numbers. For the second phase, a rapid rate of vortex decay occurs due to the onset of short-wave and long-wave vortex instabilities.⁴⁰ The onset time of long-wave instability (i.e. linking or Crow instability) depends upon the ambient turbulence intensity,³⁴ while the onset time of short-wave instability depends upon both stratification and turbulence.⁴⁰

In this appendix, a description of the TASS parametric study and a presentation of the data are summarized and the development of the TDAMP model from these results is presented (the TASS model is described in appendix B). Also included are comparisons of TDAMP predictions with eight observed cases from the 1995 Memphis wake vortex deployment.

TASS Parametric Cases

In order to determine wake vortex sensitivity to environmental conditions, three-dimensional TASS simulations are conducted with a range of values for environmental turbulence and stratification. Results from the simulations are normalized in order to eliminate dependency upon initial vortex strength.

TASS Domain, Boundary, and Initial Conditions

All TASS results used in this study assume the same fixed domain size and grid resolution. Periodic boundary conditions are assumed in all coordinate directions and ground effects are ignored. The mean ambient wind velocity is assumed zero; thus, any effects from crosswind shear are ignored. Also, the initial vortex parameters remained unchanged for all simulations.

The selected values for stratification and turbulence intensity encompass a variety of atmospheric conditions. Refer to Switzer and Proctor³² for further details about the vortex parameters, domain size and resolution, boundary conditions, stratification, and ambient turbulence generation.

Table A-1 lists the three levels of thermal stratification chosen for this parametric study. The magnitude of stratification ranges from $N^* = 1.0$, representing a very stable stratification, to $N^* = 0$, corresponding to neutral stratification.

Numerical simulations were performed with a range of turbulence intensities (Table A-2) representing values typically found in the atmospheric boundary layer. Following Han *et al*²⁶ and Switzer and Proctor³², a homogeneous isotropic turbulence field is generated prior to wake vortex injection. Vortex decay from molecular diffusion is negligible since the rotational Reynolds number (Γ_∞ / ν) is $\sim 10^7$, as is the case for atmospheric wake vortices generated by transport aircraft.

Table A-1. Ambient stratification levels used for the predictive model development.

N^*	$N (s^{-1})$	$\frac{\partial \theta}{\partial z} (^\circ C/km)$	$\frac{\partial \tau}{\partial z} (^\circ C/km)$
1.0	4.42×10^{-2}	54.2	44.4
0.5	2.21×10^{-2}	13.6	3.8
0.0	0.0	0.0	-9.8

Table A-2. Ambient turbulence intensity levels used for the predictive model development.

Turbulence Intensity	$\epsilon (m^2/s^3)$	ϵ^*
Strong	3.02×10^{-3}	0.30
Moderate	1.35×10^{-3}	0.23
Weak	4.00×10^{-5}	0.07
Very Weak	1.00×10^{-7}	0.01

Table A-3 shows the matrix of TASS runs that that were utilized in the development of the predictive models. The chosen runs give a wide variation in the turbulence intensity level for neutral stratification while addressing the stratification effects at the moderate and weak turbulence intensity levels.

Table A-3. Stratification and turbulence intensity levels used for the predictive model development.

Turbulence Intensity	Strongly Stable ($N^*=1.0$)	Moderately Stable ($N^*=0.5$)	Neutral ($N^*=0.0$)
$\epsilon^* = 0.30$			X
$\epsilon^* = 0.23$	X	X	X
$\epsilon^* = 0.07$	X	X	X
$\epsilon^* = 0.01$			X

Determination of Vortex Position and Circulation

Vortex circulation and height are diagnosed from the results of each numerical simulation as described below.

Based on the vortex position in each cross-path plain (*i.e.* y - z plain), circulation is computed for each cross-path plane according to:

$$\Gamma_r(x) = \int \int_r \zeta \, dydz.$$

The circulation is not used for any plane where the vorticity vector is in excess of 30° of the x -axis.

A 10-15 m average-circulation is computed since it represents the strength of the vortex hazard,¹³ and is assumed rather than a 5-15 m average in order to reduce measurement and modeling uncertainties due to the resolution of the vortex core.

Within each cross path plane, the average circulations is computed according to:

$$\overline{\Gamma}_i^{a,b} = \frac{\int_a^b \Gamma_r \, dr}{\int_a^b dr}$$

where $a=10 \, m$, and $b = 15 \, m$.

From the TASS data, a mean average circulation is reported for each time interval by computing a mean of the circulations from the cross-path planes:

$$\overline{\Gamma}^{a,b} = \frac{1}{N} \sum_i^N \overline{\Gamma}_i^{a,b}$$

Similarly, a mean vortex position is reported for each time interval by averaging the positions from each cross-path plane.

Predictive Model Development

Based on data from the TASS simulations described above, a set of two empirical models is proposed. The first model predicts vortex transport, while the second predicts vortex hazard. They are developed as follows.

Vortex Transport Model

The circulation at radii near the vortex separation drives the vortex descent rate. Defining Γ^* as the circulation at $r = b_o$, normalized by its initial value, the rate of change in the normalized circulation at $r = b_o$ can be modeled by:

$$\frac{d\Gamma^*}{dT} = \frac{d\Gamma_L^*}{dT} + \frac{d\Gamma_D^*}{dT} + \frac{d\Gamma_S^*}{dT} \quad (\text{A-1})$$

where the terms on the righthand side are the contributions from linking instability, turbulence diffusion, and stratification, respectively.

Based on guidance from TASS results, the change in circulation from vortex linking instability (long-wave instability) is modeled by a hyperbolic tangent function of the following form:

$$\Gamma_L^* = \frac{1}{2} \left[1 - \tanh \left(\beta_1 (T - T_L - \alpha_1) \right) \right] \quad (\text{A-2})$$

The constants β_1 and α_1 assume the values of 0.6 and 1.333, respectively. Sarpkaya's³⁴ relationship for the time to vortex linking, T_L , (fig A-1) is reproduced below:

$$\begin{aligned} T_L &= 0.8039 \varepsilon^{*3/4} & \text{for } \varepsilon^* > 0.2535 \\ T_L^{1/4} e^{(-0.7T_L)} &= \varepsilon^* & \text{for } 0.0121 < \varepsilon^* < 0.2535 \\ T_L &= -180 \varepsilon^* + 9.18 & \text{for } 0.001 < \varepsilon^* < 0.0121 \\ T_L &= -9 & \text{for } \varepsilon^* < 0.001 \end{aligned} \quad (\text{A-3})$$

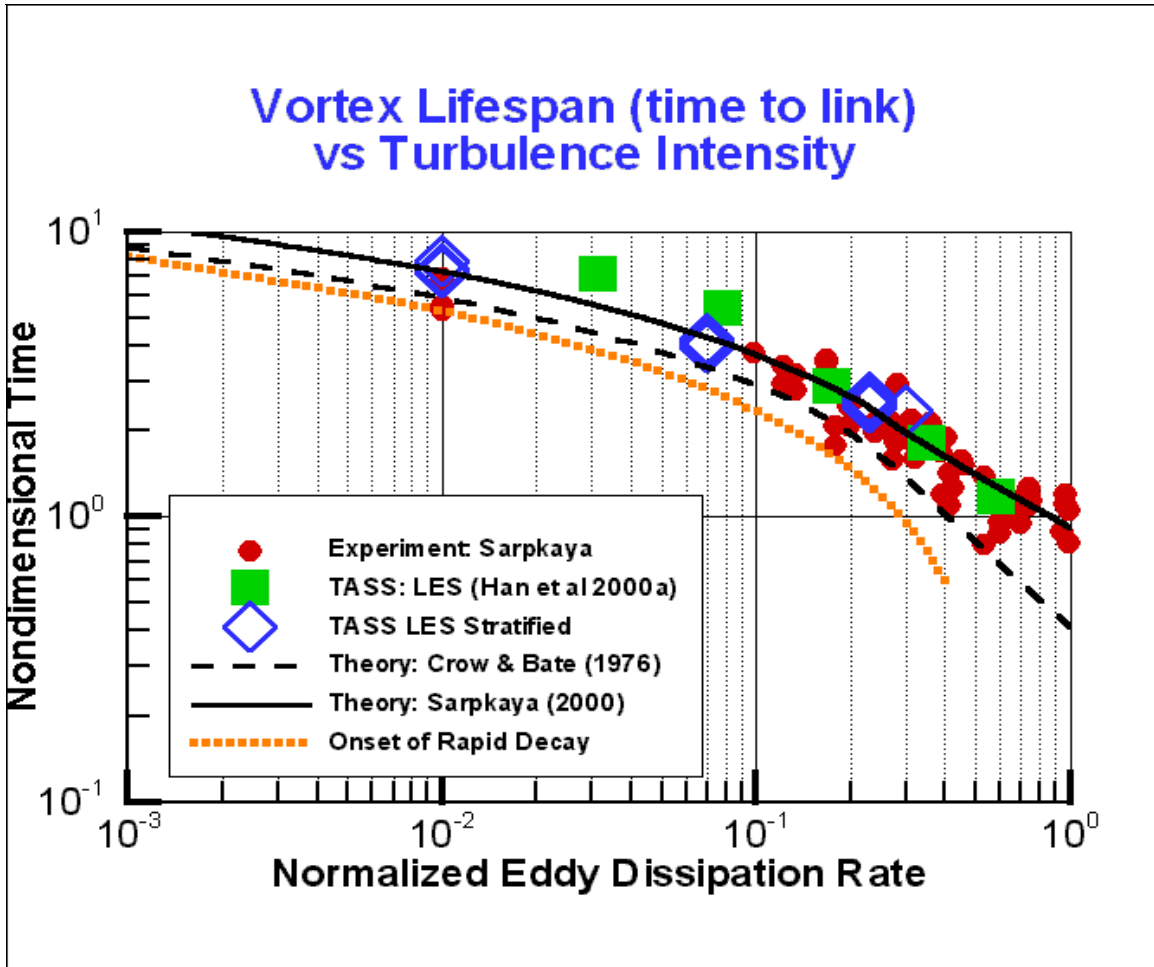


Figure A-1. Wake vortex time to link vs turbulence intensity.

In (A-2) the constant β_1 controls the slope of the decay curve, while $T - T_L - \alpha_1$ defines a nondimensional time near the beginning of rapid decay. The rate of change of Γ_L^* is:

$$\frac{d\Gamma_L^*}{dT} = -\frac{\beta_1}{2} \operatorname{sech}^2(\beta_1(T - T_L - \alpha_1)) \quad (\text{A-4})$$

Based on guidance with TASS data, the contribution from the (A-4) is limited to 62.5% of the total decay, hence:

$$\frac{d\Gamma_L^*}{dT} = -\gamma \beta_1 \operatorname{sech}^2(\beta_1(T - T_L - \alpha_1)) \quad (\text{A-5})$$

where $\gamma = 0.375$.

Turbulent diffusion assumes the model from Han *et al*²⁸:

$$\Gamma_D^* = \exp\{-c_1 \varepsilon^* T\} \quad (\text{A-6})$$

with $c_1 = 0.19$.

The associated rate of decay for (A-6) is:

$$\frac{d\Gamma_D^*}{dT} = -c_1 \varepsilon^* \Gamma_D^*$$

For ambient conditions with little or no ambient turbulence, the turbulence generated by the aircraft and wake vortices guarantee a minimal rate of decay. Therefore, in the turbulence diffusion term, ε^* is arbitrarily set to 0.08 when $\varepsilon^* < 0.08$; i.e.,

$$\frac{d\Gamma_D^*}{dT} = -c_1 \operatorname{Max}\{\varepsilon^*, 0.08\} \Gamma_D^* \quad (\text{A-7})$$

The last contribution to (A-1) comes from the change due to stratification. Following Greene³⁸:

$$\frac{d\Gamma_S^*}{dT} = -A Z N^{*2}. \quad (\text{A-8})$$

For conditions with stable stratification, the mean vortex separation can decrease with time³² causing the vortex to descend faster than if the separation remained constant. For simplicity, we have assumed that the mean vortex separation remains constant, and have empirically modified (A-8) to account for the affect on the sink rate due to change in vortex separation:

$$\frac{d\Gamma_S^*}{dT} = -A_1 Z N^{*2.5} \quad (\text{A-9})$$

where the constant, A_1 , is set equal to 0.42.

Substituting all three rate of decay terms (A-5), (A-7) and (A-9) into (A-1) gives an equation that predicts the normalized circulation at $r = b_o$:

$$\frac{d\Gamma^*}{dT} = -\gamma \beta_1 \operatorname{sech}^2(\beta_1(T - T_L - \alpha_1)) - c_1 \operatorname{Max}\{\varepsilon^*, 0.08\} \Gamma^* - A_1 Z N^{*2.5} \quad (\text{A-10})$$

If we ignore the time changes in vortex separation except how they modify (A-9), then the normalized descent rate, V^* , is equivalent to Γ^* , and

$$\frac{dV^*}{dT} = -\gamma \beta_1 \operatorname{sech}^2(\beta_1(T - T_L - \alpha_1)) - c_1 \operatorname{Max}\{\varepsilon^*, 0.08\} V^* - A_1 Z N^{*2.5} \quad (\text{A-11})$$

With T_L from (A-3), the above model predicts the vortex descent rate, assuming negligible influence from either environmental wind shear or ground effect. The vortex system initially descends at the rate of V_0 and starts to slow due to the affects of vortex linking instability, turbulence diffusion, and stratification.

The vortex height as a function of time can be integrated from $dZ/dT = V^* = \Gamma^*$, or from (A-11) as:

$$\frac{d^2Z}{dT^2} = -\gamma \beta_1 \operatorname{sech}^2(\beta_1(T - T_L - \alpha_1)) - c_1 \operatorname{Max}\{\varepsilon^*, 0.08\} \frac{dZ}{dT} - A_1 Z N^{*2.5} \quad (\text{A-12})$$

The above equation predicts the wake vortex height, Z , as a function of T , given T_L from (A-3), and with N^* and ε^* as input.

Vortex Hazard Model

A similar approach is assumed for the hazard model. The rate of change of normalized average circulation is proposed as:

$$\frac{d\bar{\Gamma}}{dT} = \frac{d\bar{\Gamma}_{SS}}{dT} + \frac{d\bar{\Gamma}_D}{dT} + \frac{d\bar{\Gamma}_S}{dT} \quad (\text{A-13})$$

where $\bar{\Gamma}$ represents the average circulation between $r = 10$ and 15 m, normalized by its initial value.

The first term on the right hand side of (A-13) represents the change in average circulation from short- and long-wave instabilities. The effect of short-wave instabilities^{41,42,43} is included since it may have a large impact on vortex decay near its core.

A model for $\bar{\Gamma}_{SS}$ similar to (A-2) is considered for representing the change in average circulation due to short- and long-wavelength instabilities:

$$\bar{\Gamma}_{SS} = \frac{1}{2} \left\{ 1 - \tanh \left[\left(\beta_2 + \beta_3 N^{*4} \right) (T - T_{SS}) - \alpha_2 \right] \right\} \quad (\text{A-14})$$

Based on TASS results, the constants β_2 , β_3 , and α_2 are set to 0.68, 0.25 and 1.875, respectively. The differences between this term and the corresponding term from the transport model (A-2) are the dependence on stratification and the dependence on T_{SS} rather than T_L . The equation for the onset of short and long wave instabilities is given in nondimensional time units as:⁴⁰

$$T_{SS} = -(1.27 \ln(\varepsilon^*) + 0.57) \exp(-1.15N^*), \text{ for } \varepsilon^* < 0.3. \quad (\text{A-15})$$

Unlike Sarpkaya's relationship for T_L described in (A-3), the above relationship depends upon stratification as well as turbulence intensity. The dependency upon stratification is necessary

since short-wavelength instabilities (and rapid decay) are induced earlier in more stable environments.⁴⁰

The rate of change of (A-14) gives:

$$\frac{d\bar{\Gamma}_{SS}}{dT} = -\frac{\beta_2 + \beta_3 N^{*4}}{2} \operatorname{sech}^2 [(\beta_2 + \beta_3 N^{*4})(T - T_{ss}) - \alpha_2] \quad (\text{A-16})$$

However, since the TASS data shows that the circulation decreases somewhat slower once the circulation has decayed to half its original value, (A-16) is modified by a time-dependent ramping function. This modification gives:

$$\frac{d\bar{\Gamma}_{SS}}{dT} = -F(T) \frac{\beta_2 + \beta_3 N^{*4}}{2} \operatorname{sech}^2 [(\beta_2 + \beta_3 N^{*4})(T - T_{ss}) - \alpha_2] \quad (\text{A-17})$$

where the ramping function is specified as:

$$F(T) = \left\{ \begin{array}{ll} 1 & T \leq T_{1/2} \\ 1 - \frac{T - T_{1/2}}{2.5} & T_{1/2} < T < T_{1/2} + 2.5 \\ 0 & T \geq T_{1/2} + 2.5 \end{array} \right\} \quad (\text{A-18})$$

In (A-18), the variable $T_{1/2}$ represents the nondimensional time that the circulation decays to half its original value; i.e., $\bar{\Gamma}(T_{1/2}) = 0.5$. Hence, the ramping function begins to decrease the contribution from (A-17) once $\bar{\Gamma}$ has decayed to half its initial value, reducing its rate to zero after 2.5 time units.

The second term on the right hand side of (A-13) represents the rate of change due to turbulence diffusion. Similar to (A-7) in the transport equation, it is represented as

$$\frac{d\bar{\Gamma}_D}{dT} = -c_2 \operatorname{Max}\{\varepsilon^*, 0.08\} \bar{\Gamma}_D \quad (\text{A-19})$$

where $c_2 = 0.22$. As in (A-7) a threshold of 0.08 is assumed in (A-19) to account for turbulence diffusion when environments are nearly laminar. Note that the rate of change of average circulation from (A-19) is slightly greater than predicted with (A-7). Hence the rate of decay from turbulence diffusion is slightly larger a smaller radii.

The remaining term in (A-13), is the rate of change of average circulation due to thermal stratification. Similar to (A-8), it is:

$$\frac{d\bar{\Gamma}_S}{dT} = -A_2 Z N^{*2} \quad (\text{A-20})$$

This term is identical to that used by Greene³⁸, except that the value for the constant is assumed as $A_2 = 0.035$. The smaller value is used since stratification (via baroclinic generation of

opposite sign vorticity) is less effective in reducing the circulation at small radii than at larger radii.

Combining the affects from the three respective terms, by substituting (A-17), (A-19), and (A-20) into (A-13) gives:

$$\frac{d\bar{\Gamma}}{dT} = -F(T) \frac{\beta_2 + \beta_3 N^{*4}}{2} \operatorname{sech}^2 \left[(\beta_2 + \beta_3 N^{*4})(T - T_{ss}) - \alpha_2 \right] - c_2 \operatorname{Max}\{\varepsilon^*, 0.08\} \bar{\Gamma}_D - A_2 Z N^{*2} \quad (\text{A-21})$$

The above equation can then be integrated to arrive at a prediction for the normalized average circulation, which represents the vortex hazard. Solution of the above equation needs Z from equation (A-12), T_{SS} from (A-15), and $F(T)$ from (A-18), as well as N^* and ε^* as input.

The above equation predicts the rate of decay of $\bar{\Gamma}$, which is related to the vortex hazard. It differs from the prediction of Γ^* from (A-10) which represents the circulation at larger vortex radii that drives vortex descent.

Predictive Model Comparisons with TASS

The above formulations and choice of constants are based on the TASS experiments listed in table A-3. Figures A-2 through A-4 show the comparisons of the vortex transport model (eq A-12) with the TASS results. In fig A-2, note that for increasing levels of turbulence the magnitudes of sink rate and depth of maximum descent are reduced. Also, the comparison across the range of turbulence intensity shows very good agreement between TASS and model data. The next two figures (A-3 and A-4) evaluate the model's ability to handle the affects of stratification at two different turbulent intensity levels. Both show a close match with the TASS data. Figures A-5 through A-7 show the comparison between the predictions with the vortex hazard model (eq A-21) and TASS results. Again the model fits nicely to the TASS data.

Although not used in the development of TDAWP, data from the TASS simulation of the JFK accident case (as described in section 5.3.3) also is included in figs A-3 and A-6 (labeled "TASS $N^*=0.257$ "). This data compares very well to the predictions based on the TDAWP model (labeled "Model $N^*=0.257$ ").

As evident from figs A-5 through A-7, TDAWP predicts a modest level of circulation decay followed by a period of more rapid decay, as is supported by TASS data. This period of rapid decay is not "stochastic,"⁴⁴ but a function of weather conditions such as turbulence and stratification.

Model results from TASS indicate that vortex descent through strong stratification can rapidly reduce circulation at larger radii, such that each member of the vortex pair becomes decoupled. Thus a vortex pair may stall, but still remain sufficiently intense with regard to vortex strength. A one-equation model would not be able to capture this effect since vortex strength and descent are computed from a uniform value for circulation; however, TDAWP can predict this behavior (cf. figs A-3 and A-6) since it relies on separate equations for prediction of descent and vortex hazard.

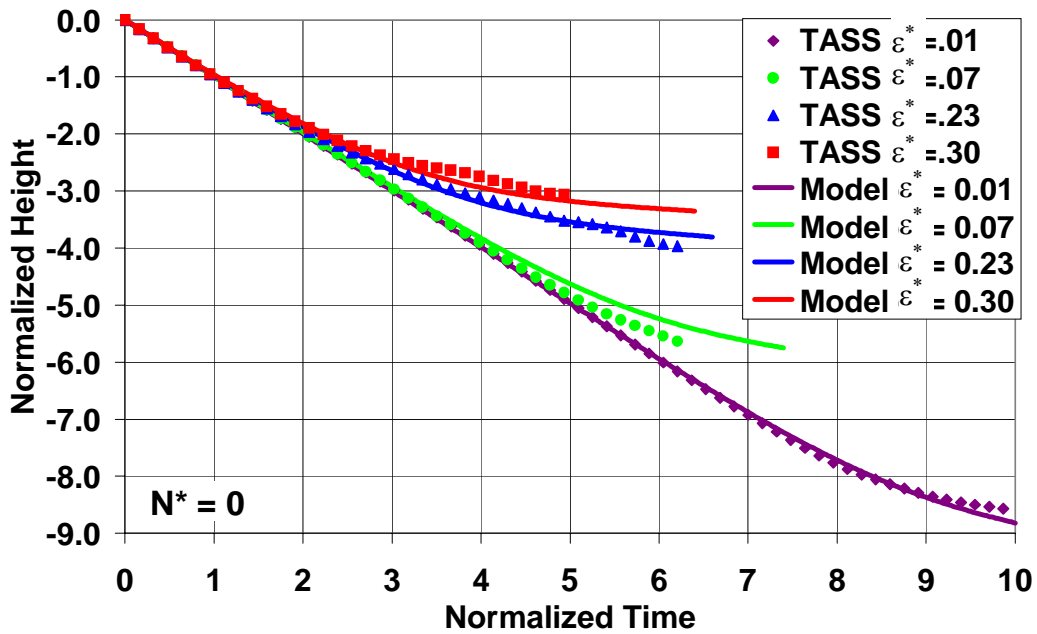


Figure A-2. Comparison of TDAWP predictive model for transport to TASS results for neutral stratification. The symbols and the lines with symbols refer to TASS and the predictive model, respectively.

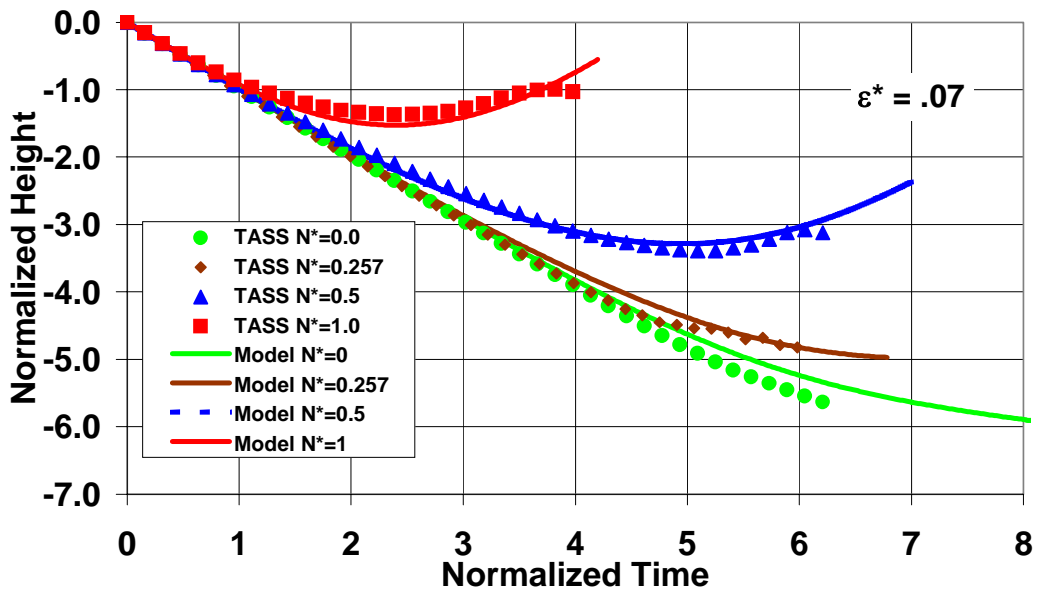


Figure A-3. Same as fig A-2, but for the weak turbulence intensity level.

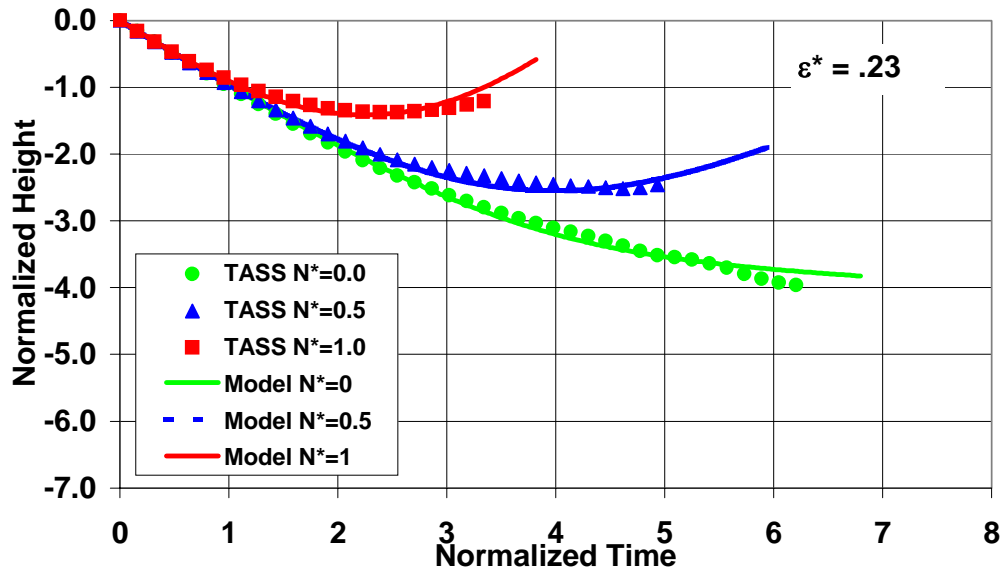


Figure A- 4. Same as fig A-3, but for the moderate turbulence intensity level.

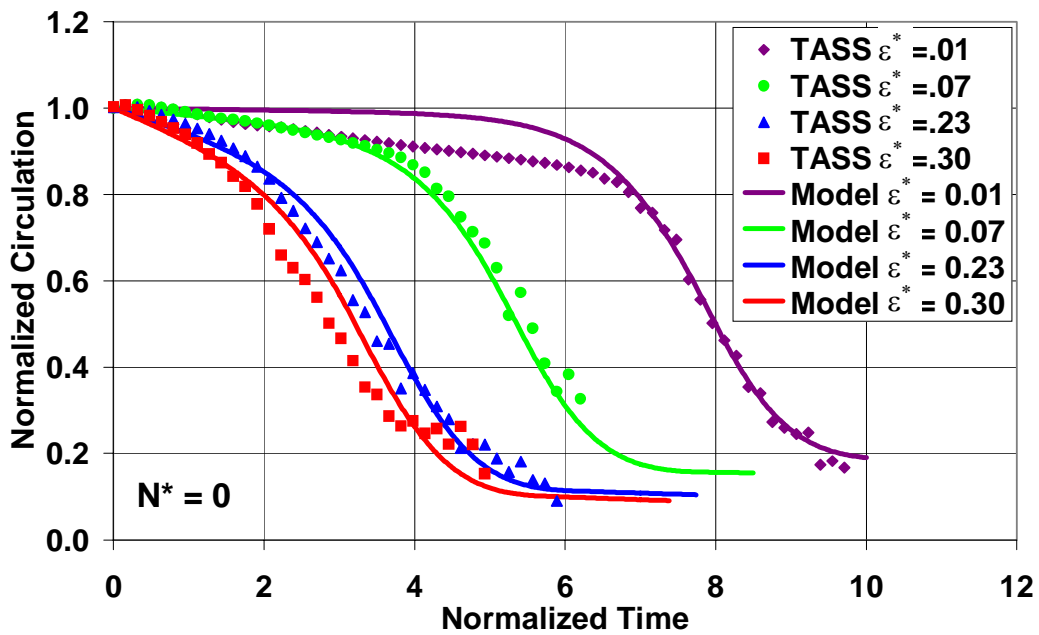


Figure A- 5. Comparison of TDAWP predictive model for hazard to TASS results for neutral stratification. The symbols and the lines with symbols refer to TASS and the predictive model, respectively.

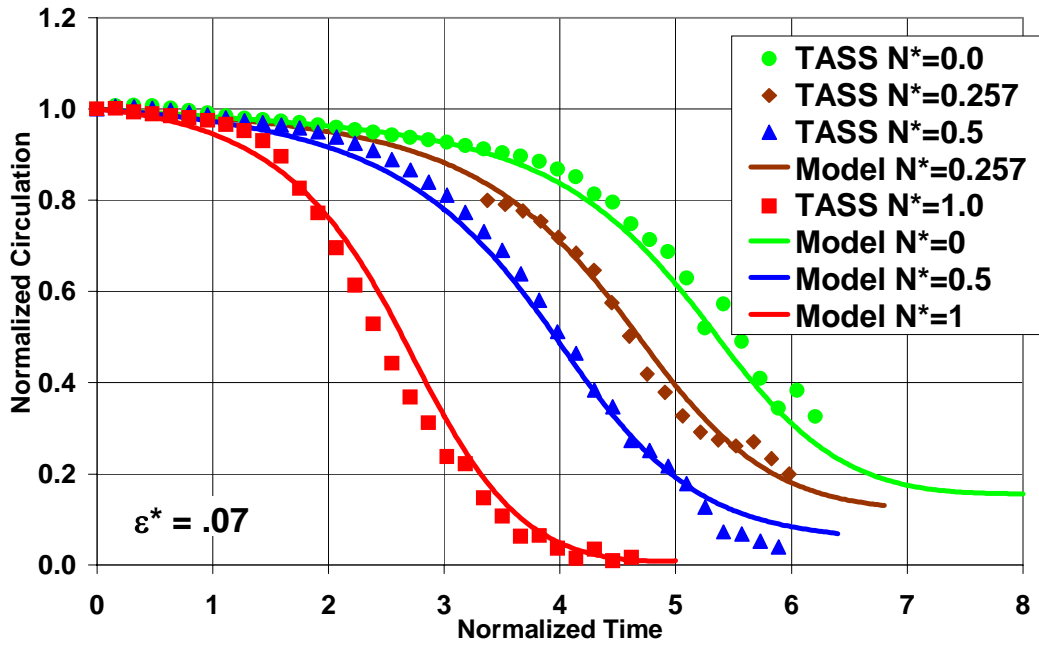


Figure A- 6. Same as fig A-5, but for the weak turbulence intensity level.

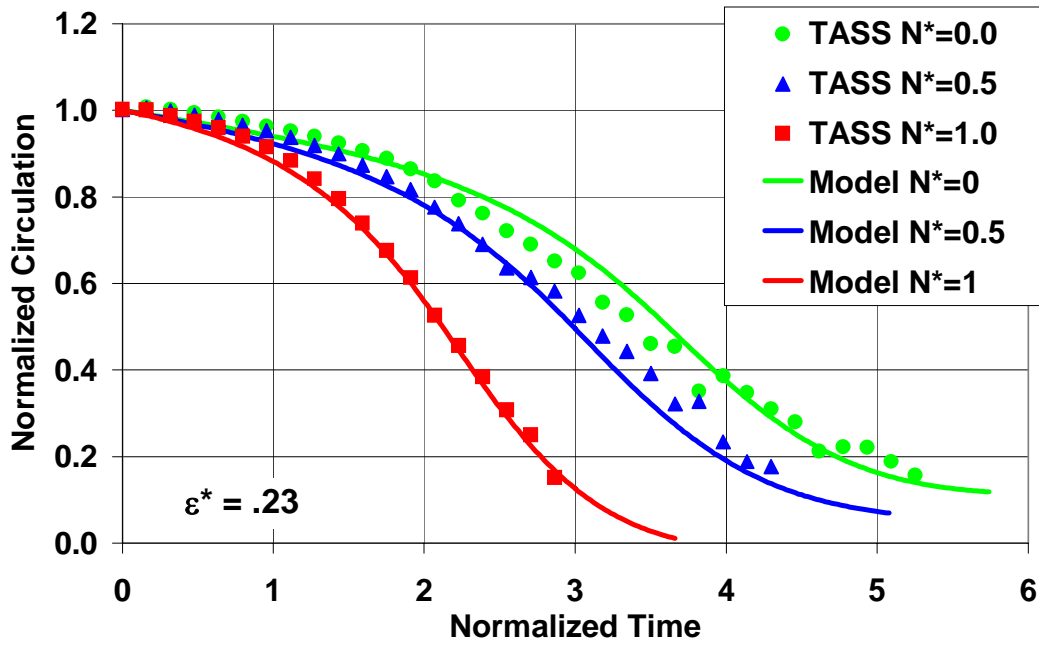


Figure A- 7. Same as fig A-6, but for the moderate turbulence intensity level.

Verification of TDAWP with Field Measurements

In order to verify that TDAWP may be a useful predictor, eight cases are taken from the AVOSS 1995 field deployment^{45,46}. As shown in table A-4, six aircraft types are used with a range of environmental conditions varying from: very light to moderate boundary-layer turbulence, and near neutral to stratified thermal stability. Cases were deliberately picked that had a minimal amount of vertical shear of the crosswind. Also, cases were chosen that were without influence from ground effect. Values for stratification were computed between the aircraft generating height (z_o) and the lowest altitude measured for the vortex. The range of magnitudes for N^* varied between 0.00 to 0.45.

Values for the eddy dissipation rate (EDR), were estimated from 15-*min* wind data as observed from a 42 *m* wind tower deployed during the field study.⁴⁷ For near neutral stratification, EDR was derived from the 40 *m* altitude level. For stable conditions, EDR was extrapolated above the tower using algorithms developed by Han *et al*⁴⁸, and averaged over the measured wake altitudes. The values were then normalized for the appropriate aircraft as shown in table A-4. The range of magnitudes for ϵ^* varied between 0.01 and 0.29.

Table A- 4. Description of cases used from Memphis field study.

Case #	Date	Time UTC	Aircraft	Γ_o (m^2s^{-1})	b_o (<i>m</i>)	z_o (<i>m</i>)	ϵ^*	N^*	Influence of Shear [†]
1238	8/15/95	5:34	Airbus 300	393	35.2	170	.066	.384	negligible
1252	8/16/95	2:57	B-757	323	29.9	185	.011	.187	light
1273	8/16/95	4:13	DC-10-30	366	39.6	170	.027	.317	moderate
1275	8/16/95	4:18	B-727-200	304	25.8	195	.018	.182	light
1456	8/24/95	5:26	Airbus 310	396	34.5	185	.028	.447	negligible
1569	8/28/95	0:05	DC-9	241	22.4	165	.120	0	negligible
1581	8/28/95	17:32	B-757	297	29.9	210	.286	0	negligible
1584	8/28/95	17:45	DC-9	254	22.4	185	.228	0	negligible

[†]Observed change in vortex drift due to vertical shear of crosswind.

Average circulation for the eight cases listed in table A-4 are depicted in fig A-8. The predictions of average circulation from *eq* (A-21) fit an upper bound to the field measurements of estimated 10-15 *m* average circulation. Note that the field data supports the model predictions of slow decay followed by a period of more rapid decay. The onset time of this rapid decay varies from $T \sim 5$ for the low-intensity turbulence cases to $T < 3$ for the cases with active daytime boundary-layer turbulence. In case with moderate ambient turbulence (cases 1581 and 1584), the change in decay rate is less obvious than in cases with weak ambient turbulence.

Similarly, predictions of vortex height *vs* time from *eq* (A-12) are compared with LIDAR measurements in fig A-9. Field data closely matches the model predictions for each case with the exceptions of Case 1252 and 1273. In these two cases the field data tends to stabilize at a

higher altitude than predicted from the model. This difference is attributed to the presence of nonlinear shear which is not accounted for in the model predictions. Case 1273, which has the strongest vertical gradient of crosswind shear, differs significantly from the model prediction for $T > 4$. From previous studies it is known that nonlinear vertical shear of the crosswind can reduce the vortex descent rate.^{20,22,49}

Summary

This appendix has presented a composite model to predict vortex transport and decay in conditions free from crosswinds and ground effects. There are two parts of this model arising from the dominance of different mechanisms at different distances from the vortex core. The models show very good agreement to TASS cases and field data.

The proposed model needs to be evaluated further before application in an operational system. In future work, the model needs to be compared and refined with LIDAR measurements of wake vortices, as previously done with Sarpkaya's²¹ model. Lastly, effects of windshear and ground effect need to be considered and incorporated into the model.

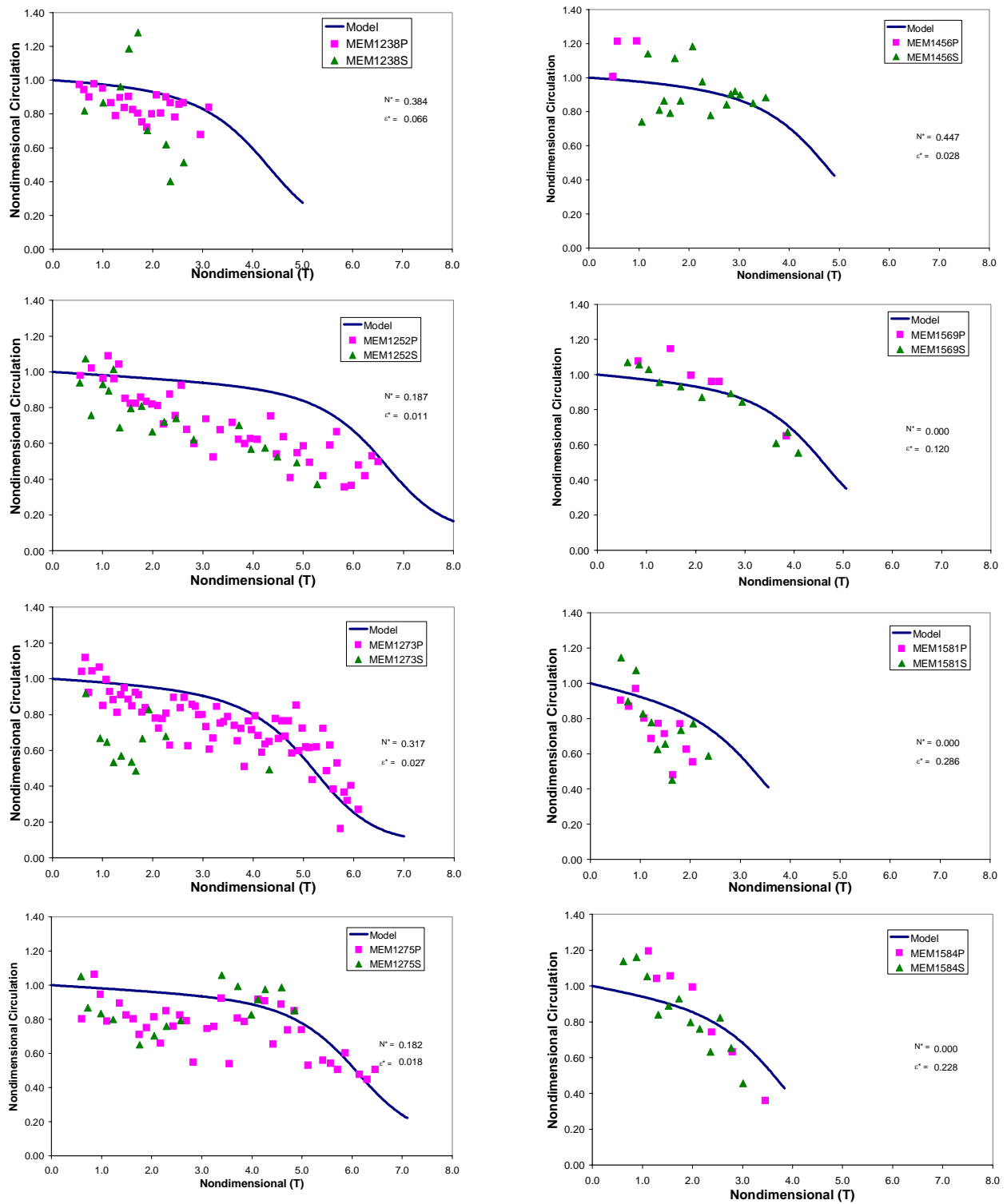


Figure A- 8. Comparison between TDAWP model predictions and Memphis field data for circulation vs time. Squares represent LIDAR estimates of port vortex while triangles represent starboard.

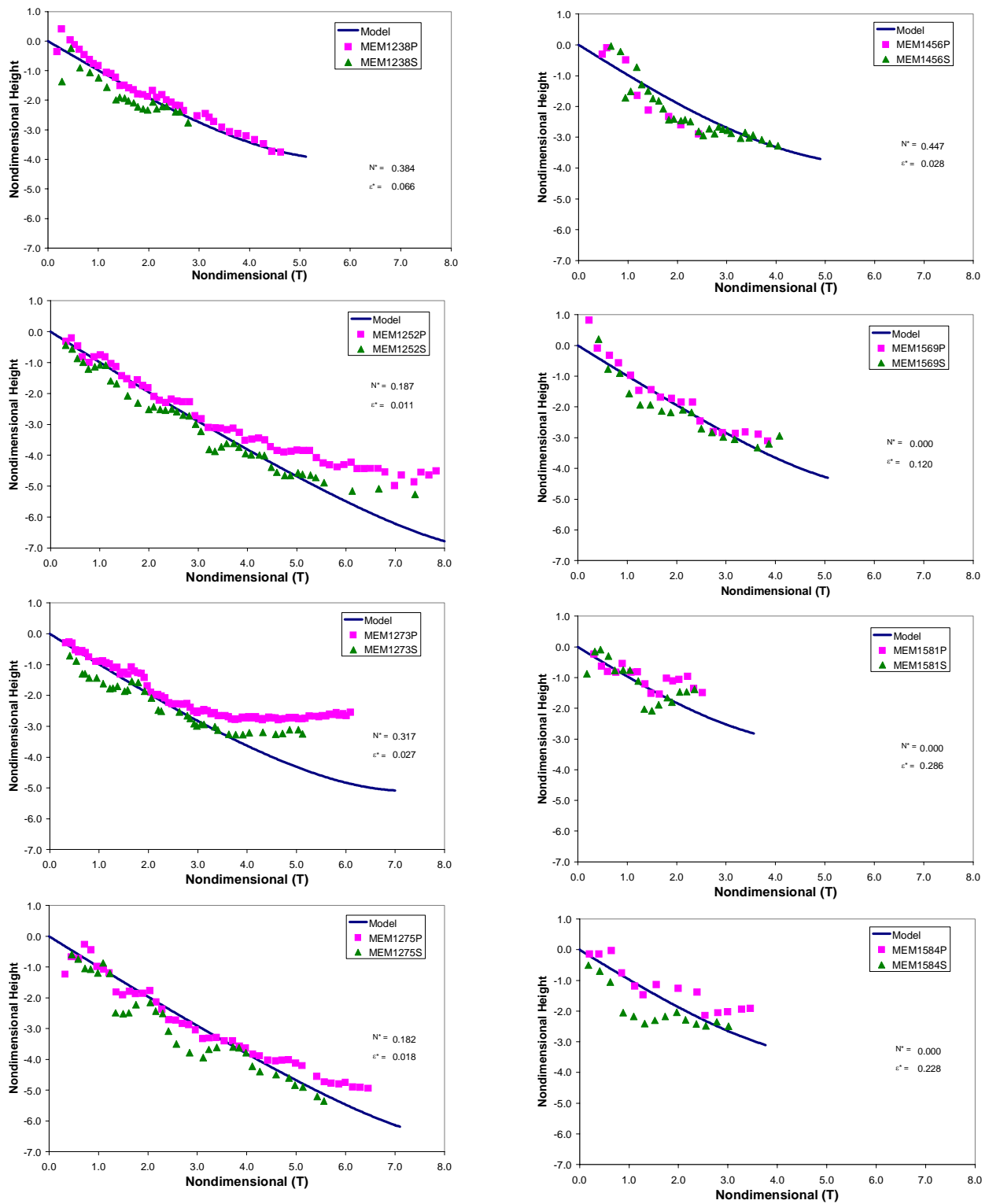


Figure A- 9. Comparison between TDAWP predictions and Memphis field data for altitude vs time. Squares represent LIDAR measurements of port vortex while triangles represent starboard vortex.

Appendix-B. Description of TASS

The Terminal Area Simulation System (TASS) is a time-split compressible, numerical model formulated within a meteorological framework.^{22,50} TASS has many sophisticated features that allow it to simulate various environmental conditions, including convective local storms, microbursts and low-level windshear, aircraft wake vortices, atmospheric boundary layer turbulence, convection-induced turbulence, urban fires, and nuclear cloud rise. It was developed by the first author almost two decades ago and has been continuously modified and updated to support NASA programs that contributed to aviation safety and increased airport capacity. It also has been used in developing certification data sets for the FAA, and has aided in reconstructing accident cases for NTSB. Previous applications of TASS are summarized in Table B-1.

Table B-1. TASS History

- Development began in 1983 for NASA/FAA Windshear Program.
- Recently applied in NASA's Wake Vortex Program for improving airport capacity.
- Currently used in NASA/FAA program to study convectively induced turbulence and improve aviation safety.
- Produced data sets for FAA certification of onboard windshear sensors.
- Produced data sets for potential certification of onboard turbulence radars.
- Supported NTSB investigation of 1994 Charlotte and 1999 Little Rock aircraft accidents.

In wake vortex applications, TASS has demonstrated good agreement with observational data;^{20, 22, 27, 28, 29, 32} and therefore, can be a useful tool for quantifying wake vortex sensitivity to atmospheric variables, as well as generating realistic velocity and temperature fields (models) at various stages of wake evolution.

The TASS model can be used in either two or three-dimensions and consists of prognostic equations: for momentum, potential temperature, water substance, and pressure deviation. Other characteristics of TASS are: 1) it has a meteorological framework, 2) its computations are LES and at high Reynolds number, and 3) it can be initialized with realistic turbulence fields. Salient features of TASS are listed in Table 1.

The TASS equation set in standard tensor notation is as follows:

Momentum:

$$\frac{\partial u_i}{\partial t} + \frac{H}{\rho_o} \frac{\partial p}{\partial x_i} = - \frac{\partial u_i u_j}{\partial x_j} + u_i \frac{\partial u_j}{\partial x_j} + g(H-1)\delta_{i3} + \frac{1}{\rho_o} \frac{\partial}{\partial x_j} \rho_o K_M \left[\frac{\partial u_i}{\partial x_j} + \frac{\partial u_j}{\partial x_i} - \frac{2}{3} \frac{\partial u_k}{\partial x_k} \delta_{ij} \right]$$

Buoyancy Term:

$$H = \left[\frac{\theta}{\theta_o} - \frac{p C_v}{P_o C_p} \right]$$

Pressure Deviation:

$$\frac{\partial p}{\partial t} + \frac{C_p P}{C_v} \frac{\partial u_j}{\partial x_j} = \rho_o g u_j \delta_{j3}$$

Thermodynamic Equation (Potential Temperature):

$$\frac{\partial \theta}{\partial t} = - \frac{1}{\rho_o} \frac{\partial \theta \rho_o u_j}{\partial x_j} + \frac{\theta}{\rho_o} \frac{\partial \rho_o u_j}{\partial x_j} + \frac{1}{\rho_o} \frac{\partial}{\partial x_j} \left[\rho_o K_H \frac{\partial \theta}{\partial x_j} \right]$$

with the *Potential Temperature* being defined as:

$$\theta = T \left(\frac{P_{oo}}{P} \right)^{\frac{R_d}{C_p}}$$

where θ is conserved for dry adiabatic processes.

In the above equations, u_i is the tensor component of velocity, t is time, p is deviation from atmospheric pressure P , T is atmospheric temperature, ρ is the air density, C_p and C_v are the specific heats of air at constant pressure and volume, g is the earth's gravitational acceleration, R_d is the gas constant for dry air, P_{oo} is a constant equivalent to 1000 millibars (10^5 pascals) of pressure. Environmental state variables are defined from the initial input sounding and are functions of height only.

The subgrid eddy viscosity is determined from a modified Smagorinsky model⁵¹ given by the following relationship for the subgrid eddy viscosity:

$$K_M = (c_s \Delta)^2 |D| (1 - \alpha_1 Ri_S - \alpha_2 Ri_R)$$

where K_M is the subgrid eddy viscosity, Δ is the filter width, D is the rate of deformation, and Ri_S and Ri_R are the Richardson numbers due to stratification and rotation, respectively. The remaining terms, $c_s=0.16$, $\alpha_1=3.0$, and $\alpha_2=1.5$ are constants. The filter width is based on the minimal resolvable scale:

$$\Delta = [2\Delta_x 2\Delta_y 2\Delta_z]^{1/3}$$

where Δ_x , Δ_y , and Δ_z are the numerical grid sizes in the respective x , y , z direction.

Time-derivative approximations for momentum and pressure are time-split explicit for computational efficiency. The convective terms in the momentum equations are approximated using 4th-order, energy-conserving, space differencing. Only light numerical filtering is applied using a 6th-order filter. Potential temperature and water substances equations are approximated with third-order accurate time and space differences with upstream-biased quadratic interpolation.⁵² The horizontal derivatives in TASS are approximated on an Arakawa-C grid.⁵³ The numerical formulation for TASS is stable for long-term integrations and is essentially free from numerical diffusion.⁵⁴

References

-
- ¹ NTSB, 2002: American Airlines, Flight 587, Airbus Industries A300-600, N14053, Belle Harbor, New York, November 12, 2001. Docket No. SA-522, National Transportation Safety Board (available at <http://www.nts.gov/events/2001/AA587/exhibits/default.htm>).
- ² Souders, C.G., and R.C. Showalter, 2002: The role of ITWS in the National Airspace System modernization: an update. Preprints, 10th Conf. On Aviation, Range, and Aerospace Meteorology, 13-16 May, Portland, Amer. Meteor. Soc., 5-8.
- ³ FAA, 1998: Description of Integrated Terminal Weather System (ITWS) weather products. Federal Aviation Administration, ITWS Program Office, 61 pp. [available at http://www1.faa.gov/ats/atb/sectors/weather/ITWS/doc_files/ProductDescription.pdf]
- ⁴ Benjamin, S.G., S.S. Weygandt, B.E. Schwartz, T.L. Smith, T.G. Smirnova, D. Kim, G. Grell, D. Devenyi, K.J. Brundage, J.M. Brown, and G.S. Manikin, 2002: The 20-km RUC in operations. Preprints, 15th Conf. on Numerical Weather Prediction, San Antonio, TX, Amer. Meteor. Soc., 379-382.
- ⁵ Kaplan, M.L., Y-L. Lin, J.J. Charney, K.D. Pfeiffer, D.S. DeCroix, and R.P. Weglarz, 2000: A Terminal Area PBL Prediction System at Dallas-Fort Worth and its application in simulating diurnal PBL jets. *Bull. Amer. Meteor. Soc.*, **81**, 2179-2204.
- ⁶ *Air Traffic Controller's Handbook*, FAA Order# 7110.65N.
- ⁷ Rutishauser, D., 2003: Progress towards the investigation of technical issues relevant to the design of an Aircraft Wake Vortex Avoidance System (WakeVAS). 21st AIAA Applied Aerodynamic Conference, June 23-26, Orlando, FL, AIAA-2003-3808, 6 pp. [available at <http://techreports.larc.nasa.gov/ltrs/ltrs.html>]
- ⁸ Crow, S.C., 1970: Stability theory for a pair of trailing vortices. *AIAA Journal*, **8**, 2172-2179.
- ⁹ Condit P.M. and P.W. Tracy, 1971: Results of the Boeing Company wake turbulence test program. *Aircraft Wake Turbulence and Its Detectio*. Plenum Press, J.H Olsen, A. Goldberg, and M. Rogers editors, 473-508.
- ¹⁰ Garodz, L.J., and K.L. Clawson, 1993: Vortex wake characteristics of B757-200 and B767-200 aircraft using the tower fly-by technique, Volumes 1 and 2. NOAA Tech. Memo. ERL-ARL-199.
- ¹¹ Delisi, D.P., G.C. Greene, R.E. Robins, D.C. Vicroy, and F.Y. Wang, 2003: Aircraft wake vortex core size measurements. 21st AIAA Applied Aerodynamic Conference, June 23-26, Orlando, FL, AIAA-2003-3811, 9 pp.
- ¹² Burnham, D.C., and J.N. Hallock, 1982: Chicago Monostatic Acoustic Vortex Sensing System, Volume IV: wake vortex decay. Report No. DOT-TSC-FAA-79-18 IV, 206 pp.
- ¹³ Hinton, D.A., and C.R. Tatnall, 1997: A candidate wake vortex strength definition for application to the NASA aircraft vortex spacing system (AVOSS). NASA TM-110343, 35 pp. [available at <http://techreports.larc.nasa.gov/ltrs/ltrs.html>]
- ¹⁴ Hinton, D.A., 1995: Aircraft Vortex Spacing System (AVOSS) conceptual design. NASA TM-110184, 27 pp.
- ¹⁵ Chambers, J.R., 2003: *Concept to Reality: Contributions of the NASA Langley Research Center to U.S. Civil Aircraft of the 1990s*. NASA SP-2003-4529, 209-231.

-
- ¹⁶ Perry, R.B., D.A. Hinton, and R.A. Stuever, 1997: NASA wake vortex research for aircraft spacing. 35th Aerospace Sciences Meeting & Exhibit, AIAA 97-0057, 9 pp. [available at <http://techreports.larc.nasa.gov/ltrs/ltrs.html>]
- ¹⁷ Hinton, D.A., J.K. Charnock, D.R. Bagwell, D. Grigsby, 1999: NASA aircraft vortex spacing system development status. 37th Aerospace Sciences Meeting & Exhibit, January 11-14, Reno, NV, AIAA 99-0753, 17 pp. [available at <http://techreports.larc.nasa.gov/ltrs/ltrs.html>]
- ¹⁸ O'Connor, C.J.; and D.K. Rutishauser, 2001: Enhanced airport capacity through safe, dynamic reductions in aircraft separation NASA's Aircraft Vortex Spacing System. *Journal of Air Traffic Control*, **43**, 4-10.
- ¹⁹ Rutishauser, D., G. Lohr, D. Hamilton, R. Powers, B. McKissick, C. Adams, and E. Norris, 2003: Wake Vortex Advisory System (WakeVAS) concept of operations. NASA TM-2003-212176, 27 pp. [available at <http://techreports.larc.nasa.gov/ltrs/ltrs.html>]
- ²⁰ Proctor, F.H., 1998: The NASA-Langley wake vortex modelling effort in support of an operational aircraft spacing system. Invited paper, 36th Aerospace Sciences Meeting & Exhibit, 12-15 January, Reno, NV, AIAA 98-0589, 19 pp. [available at <http://techreports.larc.nasa.gov/ltrs/ltrs.html>]
- ²¹ Sarpkaya, T., Robins, R. E., and D.P. Delisi, 2001: Wake-vortex eddy-dissipation model predictions compared with observations. *Journal of Aircraft*, **38**, 687-692.
- ²² Proctor, F.H., 1996: Numerical simulation of wake vortices measured during the Idaho Falls and Memphis field programs. 14th AIAA Applied Aerodynamics Conference, Proceedings, Part-II, 17-20 June, New Orleans, LA, AIAA-96-2496, 943-960. [available at <http://techreports.larc.nasa.gov/ltrs/ltrs.html>]
- ²³ Buck, B.K., and S.G. Velotas, 2003: Development of an aircraft approach & departure atmospheric profile generation algorithm. AeroTech Research Inc, Hampton VA, Report ATR-2003-16002.
- ²⁴ Robins, R.E., and D.P. Delisi, 2002: NWRA AVOSS wake vortex prediction algorithm version 3.3.1. NASA Report No. CR-2002-21746, 64 pp. [available at <http://techreports.larc.nasa.gov/ltrs/ltrs.html>]
- ²⁵ Robins, R.E., and D.P. Delisi, 2002: Wake vortex algorithm scoring results. NASA Report No. CR-2002-21745, 44 pp. [available at <http://techreports.larc.nasa.gov/ltrs/ltrs.html>]
- ²⁶ Han, J., Y-L. Lin, D.G. Schowalter, S.P. Arya, and F.H. Proctor, 2000: Large eddy simulation of aircraft wake vortices within homogeneous turbulence: Crow instability. *AIAA Journal* **38**, 292-300.
- ²⁷ Proctor, F.H., and J. Han, 1999: Numerical study of wake vortex interaction with the ground using the Terminal Area Simulation System. 37th Aerospace Sciences Meeting & Exhibit, January 11-14, Reno, NV, AIAA-99-0754, 12 pp. [available at <http://techreports.larc.nasa.gov/ltrs/ltrs.html>]
- ²⁸ Han, J., Y.-L. Lin, S.P. Arya, and F.H. Proctor, 2000: Numerical study of wake vortex decay and descent within homogeneous turbulence. *AIAA Journal*, **38**, 643-656.
- ²⁹ Shen, S., F. Ding, J. Han, Y-L, Lin, S.P. Arya, and F.H. Proctor, 1999: Numerical modeling studies of wake vortices: Real case simulations. 37th Aerospace Sciences Meeting & Exhibit, January 11-14, Reno, NV, AIAA-99-0755, 16 pp. [available at <http://techreports.larc.nasa.gov/ltrs/ltrs.html>]
- ³⁰ Vincent, A. and M. Meneguzzi, 1991: The spatial structure and statistical properties of homogeneous turbulence. *Journal of Fluid Mechanics*, **225**, 1-20.

-
- ³¹ Kolmogorov, A.N., 1941: The local structure of turbulence in incompressible viscous fluid for very large Reynolds number. *Dokl. Akad. Nauk SSSR*, **30**, 9-13.
- ³² Switzer, G., and F.H. Proctor, 2000: Numerical study of wake vortex behavior in turbulent domains with ambient stratification. 38th Aerospace Sciences Meeting & Exhibit, January 10-13, Reno, NV, AIAA-2000-0755, 14 pp. [available at <http://techreports.larc.nasa.gov/ltrs/ltrs.html>]
- ³³ Saffman, P.G., 1992: *Vortex Dynamics*. Cambridge University Press, 311 pp.
- ³⁴ Sarpkaya, T., 2000: New model for vortex decay in the atmosphere. *AIAA Journal*, **37**, 53-61.
- ³⁵ Crow, S.C. and E.R. Bate, 1976: Lifespan of trailing vortices in a turbulent atmosphere. *Journal of Aircraft*, **13**, 476-482.
- ³⁶ Liu, H.T., 1992: Effects of ambient turbulence on the decay of trailing vortex wake. *Journal of Aircraft*, **29**, 255-262.
- ³⁷ Switzer, G.F., and F.H. Proctor, 2002: Wake vortex prediction models for decay and transport within stratified environments. 40th Aerospace Sciences Meeting & Exhibit, 14-17 January, Reno, NV, AIAA-2002-0945, 6 pp. [available at <http://techreports.larc.nasa.gov/ltrs/ltrs.html>]
- ³⁸ Greene, G.C., 1986: An approximate model of vortex decay in the atmosphere. *Journal of Aircraft*, **23**, 566-573.
- ³⁹ Holzaphel, F., 2003: Probabilistic two-phase wake vortex decay and transport model. *Journal of Aircraft*, **40**, 323-331.
- ⁴⁰ Proctor, F.H., and G.F. Switzer, 2000: Numerical simulation of aircraft trailing vortices. Preprints of the 9th Conference on Aviation, Range and Aerospace Meteorology, Orlando, FL, Amer. Meteor. Soc., 511-516. [available at <http://techreports.larc.nasa.gov/ltrs/ltrs.html>]
- ⁴¹ Leweke, T., and C.H.K. Williamson, 1998: Cooperative elliptic instability of a vortex pair. *J. Fluid Mech.*, **360**, 85-119.
- ⁴² Sipp, D., 2000: Weakly nonlinear saturation of short-wave instabilities in a strained Lamb-Oseen vortex. *Physics of Fluids*, **12**, 1715-1729.
- ⁴³ Delisi, D.P., and R.E. Robins, 2000: Short-scale instabilities in trailing wake vortices in a stratified fluid. *AIAA Journal*, **38**, 1916-1923.
- ⁴⁴ Spalart, P.R., 1998: Airplane trailing vortices. *Ann. Rev. Fluid Mech.*, **30**, 107-138.
- ⁴⁵ Campbell, S.D., T.J. Dasey, R.E. Freehart, R.M. Heinrichs, M.P. Matthews, G.H. Perras, and G.S. Rowe, 1997: Wake vortex measurement program at Memphis, TN, data guide," Project Report: NASA/L-2, January, (also in NASA CR-201690, April 1997).
- ⁴⁶ NASA Langley Research Center, 1997: Memphis 1994-95 Wake Vortex Data Set, Version 1.2, June, Compact Disc.
- ⁴⁷ Perras, G. H., and T.J. Dasey, 2000: Turbulence climatology at Dallas/Ft. Worth (DFW) Airport—Implications for a departure wake vortex spacing system. Project Report NASA/L-4, 33 pp.
- ⁴⁸ Han, J., S. Shen, S.P. Arya, and Y.-L. Lin, 2000: An estimation of turbulent kinetic energy and energy dissipation rate based on atmospheric boundary layer similarity theory. NASA Contract Report No. CR-2000-210298, 35 pp. [available at <http://techreports.larc.nasa.gov/ltrs/ltrs.html>]
- ⁴⁹ Zheng, Z.C. and K. Baek, 1999: Inviscid interactions between wake vortices and shear layers. *AIAA Journal*, **36**, 477-480.

⁵⁰ Proctor, F.H., 1987: The Terminal Area Simulation System. Volume I: theoretical formulation. NASA Contractor Report No. CR-4046, 176 pp.

⁵¹ Smagorinsky, J., 1963: General circulation experiments with the primitive equations: 1. the basic experiment. *Mon. Wea. Rev.*, **93**, 727-768.

⁵² Leonard, B.P., 1979: A stable and accurate convective modelling procedure based on quadratic upstream interpolation. *Comp. Meth. Appl. Mech. Eng.*, **19**, 59-98.

⁵³ Haltiner, G.J. and Williams, R.T., 1980: *Numerical Prediction and Dynamic Meteorology*. Second Edition, John Wiley & Sons, 226-230.

⁵⁴ Switzer, G.F., 1996: Validation tests of TASS for application to 3-D vortex simulations. NASA Contractor Report No. CR-4756, 45 pp. [available at <http://techreports.larc.nasa.gov/ltrs/ltrs.html>]

REPORT DOCUMENTATION PAGE				Form Approved OMB No. 0704-0188	
<p>The public reporting burden for this collection of information is estimated to average 1 hour per response, including the time for reviewing instructions, searching existing data sources, gathering and maintaining the data needed, and completing and reviewing the collection of information. Send comments regarding this burden estimate or any other aspect of this collection of information, including suggestions for reducing this burden, to Department of Defense, Washington Headquarters Services, Directorate for Information Operations and Reports (0704-0188), 1215 Jefferson Davis Highway, Suite 1204, Arlington, VA 22202-4302. Respondents should be aware that notwithstanding any other provision of law, no person shall be subject to any penalty for failing to comply with a collection of information if it does not display a currently valid OMB control number. PLEASE DO NOT RETURN YOUR FORM TO THE ABOVE ADDRESS.</p>					
1. REPORT DATE (DD-MM-YYYY) 01- 04 - 2004		2. REPORT TYPE Technical Memorandum		3. DATES COVERED (From - To)	
4. TITLE AND SUBTITLE Meteorology and Wake Vortex Influence on American Airlines FL-587 Accident			5a. CONTRACT NUMBER		
			5b. GRANT NUMBER		
			5c. PROGRAM ELEMENT NUMBER		
6. AUTHOR(S) Fred H. Proctor, David W. Hamilton, David K. Rutishauser, and George F. Switzer			5d. PROJECT NUMBER		
			5e. TASK NUMBER		
			5f. WORK UNIT NUMBER 23-137-30-10		
7. PERFORMING ORGANIZATION NAME(S) AND ADDRESS(ES) NASA Langley Research Center Hampton, VA 23681-2199			8. PERFORMING ORGANIZATION REPORT NUMBER L-18371		
9. SPONSORING/MONITORING AGENCY NAME(S) AND ADDRESS(ES) National Aeronautics and Space Administration Washington, DC 20546-0001			10. SPONSOR/MONITOR'S ACRONYM(S) NASA		
			11. SPONSOR/MONITOR'S REPORT NUMBER(S) NASA/TM-2004-213018		
12. DISTRIBUTION/AVAILABILITY STATEMENT Unclassified - Unlimited Subject Category 03 Availability: NASA CASI (301) 621-0390 Distribution: Standard					
13. SUPPLEMENTARY NOTES An electronic version can be found at http://techreports.larc.nasa.gov/ltrs/ or http://ntrs.nasa.gov					
14. ABSTRACT The atmospheric environment surrounding the crash of American Airlines Flight 587 is investigated. Examined are evidence for any unusual atmospheric conditions and the potential for encounters with aircraft wake vortices. Computer simulations are carried out with two different vortex prediction models and a Large Eddy Simulation model. Wind models are proposed for studying aircraft and pilot response to the wake vortex encounter.					
15. SUBJECT TERMS Aircraft wake vortices, aviation safety, aircraft accidents, large eddy simulation, turbulence, wake vortex models, Crow instability					
16. SECURITY CLASSIFICATION OF:			17. LIMITATION OF ABSTRACT	18. NUMBER OF PAGES	19a. NAME OF RESPONSIBLE PERSON
a. REPORT	b. ABSTRACT	c. THIS PAGE			STI Help Desk (email: help@sti.nasa.gov)
U	U	U	UU	60	19b. TELEPHONE NUMBER (Include area code) (301) 621-0390